Conductor and joint test results of JT-60SA CS and EF coils using the NIFS test facility

Conductor and joint test results of JT-60SA CS and EF coils using the NIFS test facility

Tetsuhiro Obana[a]*, Kazuya Takahata[a], Shinji Hamaguchi[a], Kaname Kizu[b], Haruyuki Murakami[b], Hirotaka Chikaraishi[a], Hiroki Noguchi[a], Takashi Kobuchi[a], Sadatomo Moriuchi[a], Shinsaku Imagawa[a], Toshiyuki Mito[a], Katsuhiko Tsuchiya[b], Kyohei Natsume[b], Kiyoshi Yoshida[b]
Kazuhiro Nomoto[c], and Tae-hyun Kim[c]

National Institute for Fusion Science[a], 322-6 Oroshi, Toki, Gifu, 509-5292 Japan
Japan Atomic Energy Agency[b], 801-1 Mukoyama, Naka, Ibaraki, 311-0193, Japan
Mitsubishi Electric[c], 1-1-2 Wadasaki, Hyogo-ku, Kobe, Hyogo, 652-8555, Japan

*Corresponding author. Tel.: +81 572 58 2137 ; fax: +81 572 58 2616
E-mail address: obana.tetsuhiro@LHD.nifs.ac.jp (T. Obana)

Abstract

In 2007, JAEA and NIFS launched the test project to evaluate the performance of cable-in-conduit (CIC) conductors and conductor joints for the JT-60SA CS and EF coils. In this project, conductor tests for four types of coil conductor and joint tests for seven types of conductor joint have been conducted for the past eight years using the NIFS test facility. As a result, the test project indicated that the CIC conductors and conductor joints fulfill the design requirement for the CS and EF coils. In addition, the NIFS test facility is expected to be utilized as the test facility for the development of a conductor and conductor joint for the purpose of the DEMO nuclear fusion power plant, provided that the required magnetic field strength is within 9 T.

Keywords:

JT-60SA, Cable-in-conduit (CIC) conductor, Current sharing temperature (Tcs) measurement, Joint resistance measurement, Test facility

1. Introduction

The JT-60 tokamak is being upgraded to an advanced superconducting tokamak referred to as the JT-60 super advanced (JT-60SA) at the Japan Atomic Energy Agency (JAEA) Naka site in Japan. [1－4]. The JT-60SA magnet system consists of a central solenoid (CS) coil, 18 toroidal field (TF) coils, and six plasma equilibrium (EF) field coils as illustrated in Fig. 1. Nb_3Sn cable-in-conduit (CIC) conductors are used for the CS coil, and NbTi CIC conductors are used for the TF and EF coils. JAEA was taking charge of conductor production for the CS and EF coils, and the conductor production began from 2008 at the Naka site [1,5].

In 2007, the collaborative project between JAEA and the National Institute for Fusion Science

(NIFS) was launched to evaluate the performance of the CIC conductors and conductor joints using a conductor test facility in NIFS [5,6]. Conductor tests for four types of coil conductor and joint tests for seven types of conductor joints have been conducted for the past eight years, as listed in Table 1. Tables 2 and 3 give the overviews of the conductor and joint test results, respectively. In this paper, all of the conductor and joint test results are summarized, and those test results are discussed for the conductor and joint development aiming for the DEMO nuclear fusion power plant.

2. NIFS test facility

Two test facilities of NIFS were used to conduct the performance evaluation tests of conductors and joints for JT-60SA CS and EF coils.

2.1. Test facility for large superconducting conductors

The test facility for large superconducting conductors was constructed in 1992 to develop a large aluminum stabilized superconductor for helical coils [7] and a CIC conductor for poloidal coils [8] installed in the large helical device (LHD) [9,10]. Characteristics of the superconductors immersed in liquid helium (LHe) were investigated under a maximum magnetic field of 9 T, generated by a superconducting split coil, the outer diameter of which is 907 mm. The available test space is the gap of the split coil, which is 550 × 100 mm. Fig. 2 shows the magnetic field distribution of the split coil. In addition, a DC power supply, consisting of three 25 kA unit banks, enables the superconductor to be excited up to 75 kA in the test facility [11]. The test facility is also equipped with current leads capable of carrying up to 100 kA [12].

In 2007, the test facility was modified to deal with testing of the CIC conductors for JT-60SA [6]. Fig. 3 shows the schematic view of the modified test facility. Supercritical helium (SHe) cooling lines were newly assembled with transfer tubes and a heat exchanger to flow SHe in the conductor sample. In the conductor sample, the cooling pipe at the inlet was equipped with film heaters to control the SHe temperature. A thermal insulation vessel was additionally installed inside the gap of the split coil to make a test space where the conductor sample can be installed in a gas helium atmosphere instead of LHe. The vessel, which is made of a stainless steel (SS) 316L, has a double-walled structure. Gas nitrogen was filled inside the double wall at room temperature and atmospheric pressure. During cool down, the filled nitrogen was solidified, and the space in the double wall was evacuated.

Cooling curves of a CIC conductor sample during the cooling down are shown in Fig. 4. Initially, pressurized gas helium, cooled by liquid nitrogen through a heat exchanger in the refrigerator, was supplied to the conductor sample. After 25 hours from the start of the cooling down, turbines in the refrigerator started operating. Finally, the conductor sample was cooled to about 5 K [6]. It took about 30 hours from room temperature to about 5 K. After the modification, the test facility can accommodate the testing of CIC conductor as well as that of superconductors immersed in LHe.

2.2. Test facility for middle-sized superconducting conductors

Fig. 5 shows a schematic view of the test facility for middle-sized superconducting conductors. This test facility is equipped with a superconducting split coil the outer diameter of which is 360 mm, which can generate a maximum

magnetic field of 8 T. The magnetic field distribution is shown in Fig. 6. In addition, the test facility comprises current leads capable of carrying up to 20 kA and a DC power supply enabling a sample to be excited up to 30 kA.

This facility was used to test the EF joint samples as described in section 5 [13]. A joint sample was installed in the test facility through the bore of a superconducting split coil. The joint region of the joint sample was located inside the coil bore as shown in Fig. 5. The available test space is the inside of the coil bore, which is φ90 mm. The joint sample and the split coil were connected mechanically using a SS support to prevent movement of the joint sample from electromagnetic force. In addition, the joint sample and the split coil were immersed in LHe.

3. Conductor tests for EF coil

3.1. Conductor test samples

As a conductor test sample for the EF coil, three types of conductors were used: a prototype, EF-H, and EF-L. Fig. 7 shows the cross-section of the conductors, and the major parameters of the conductors are listed in Table 4. The prototype conductor was fabricated and tested to confirm the capability of the NIFS test facility for qualification tests of real conductors, which are the EF-H and EF-L conductors. In addition, the validities of the conductor design concept and the conductor fabrication method were evaluated through the prototype conductor. For the samples of the EF-H and EF-L conductors, the qualification tests were conducted to predict the superconducting performance of fabricated conductors before mass production of real conductors.

Each conductor is a NbTi cable-in-conduit (CIC) conductor with a SS316L jacket and central spiral channel. Cables of the prototype and EF-H conductors are composed only of NbTi strands, and a cable of the EF-L conductor is composed of NbTi strands and copper wires. In terms of reduction of AC loss, the surface of the NbTi strands are plated with nickel (Ni). Additionally, SS sub-wrapping tapes are used for the prototype conductor. In the EF-H and EF-L conductors, the twist pitch of the cable is shortened and the void fraction of the conductor is increased instead of using the sub-wrapping tapes.

The fabrication process of these conductors are illustrated in Fig. 8. Jackets with unit length of 13 m are butt-welded to a long length jacket. After that, a cable is pulled into the long jacket using a winch. Finally, the circular cross-section of the cable with the jacket is formed into the square cross-section using a compaction machine.

Figs. 9 and 10 show the schematic view and photograph of the test conductor sample. The configuration of the sample is racket-shaped with the diameter of 300 mm. In the conductor test, the sample is set in the position where the center of the sample's circular part is consistent with that of the split coil, as shown in Fig. 3. The sample at the circular section, which is longer than the final twist pitch, is subjected to maximum magnetic field generated by the split coil. For Tcs measurements and stability tests, voltage taps are mainly attached on the conduit at the circular section. An inlet pipe for SHe is connected to the straight part of the sample. Details of the conductor production and the sample are described in Refs. [5, 14].

3.2. Measurements of current sharing temperature

Using the test facility for large superconducting conductors, the measurements of current sharing temperature (Tcs) for three samples were conducted. In the measurements, the SHe temperature at the inlet pipe was increased gradually

while keeping the SHe mass flow fixed. Conductor current and external field were constant. The Tcs criteria was determined to be 10 μV/m.

Fig. 11 shows the Tcs measurement results of the prototype conductor with predictive values from NbTi strand critical value. Each magnetic field includes an external field by the split coil and a self field by the conductor sample. A slight degradation of superconducting performance was observed in the prototype conductor [5]. The reason for the degradation is not yet understood. However, the result was within permissible range. The result indicated that the conductor design concept and the conductor fabrication method are valid, and the test facility of NIFS is suitable for the qualification tests of real conductors.

The Tcs measurement results of EF-H and EF-L conductor samples are shown in Figs. 12 and 13. The required Tcs of these conductors are 5.82 K at 6.2 T for the EF-H conductor and 6.14 K at 4.8 T for the EF-L conductor respectively in the case that the operating current is 20 kA. Both conductor samples fulfilled the requirements and almost agreed with predictive values from NbTi strand critical current. As a result, mass production of the EF-H and EF-L conductors was launched [14].

3.3. Stability tests

To evaluate a stability margin of EF conductors under several operating conditions, stability tests were conducted using the conductor test samples mounted by an induction heater [15, 16]. The configuration of the induction heater is a solenoid coil wound with a copper wire, and the coil length is 30 mm. As shown in Fig. 14, the inductive heater was mounted on the conduit at the circular section. The inductive heater was connected to a capacitor. Input energy for a conductor test sample was controlled by adjusting an initial charging voltage of the capacitor. Fig. 15 shows the current waveforms of the inductive heater under several magnetic fields. The current waveforms correspond to the heat input, so that the heat input was nearly completed within about 5 ms.

In the estimation of the heat input, a finite element analysis was conducted using a model assuming the test conductor sample with the inductive heater. The current waveform of the inductive heater in the analysis was based on the experimental results. Details of the model is described in Ref. [15]. To confirm the validation of the model, analysis results using the model were compared with calibration test results using the 200 mm long prototype conductor with the induction heater. In addition, analysis results were compared with the heat input test results, which are the input energy obtained from the measured temperature rise of SHe flowing inside the test conductor samples when the induction heater was operated. Consequently, the analysis results were in good agreement with those test results. The details of the calibration test and heat input test are described in Ref. [15]

Fig. 16 shows the relation between minimum quench energy (MQE) and temperature margin for the conductor test samples under various test conditions. In the measurements, the inlet pressure of SHe was about 0.6 MPa. The mass flow rates of SHe were about 4.0 g/s for the prototype and EF-L conductor test samples and about 5.0 g/s for the EF-H conductor test sample, respectively. As shown in Fig. 16, the MQE of the samples increases as the temperature margin is increased except for the prototype at the operating current of 30 kA. This test result of the prototype conductor is discussed in section 7.2.

The relation between MQE and mass flow rate for the EF-L conductor test sample is shown in Fig. 17. The test conditions are as follows: the magnetic field is 4.0 T, the operating current is 20 kA, the temperature margin is 0.2 K, and the inlet pressure is about 0.6 MPa. The MQE increases linearly with an increase of the mass flow rate. Compared to the changing rate of mass flow rate for MQE, that of the temperature margin has a great impact on MQE.

Fig. 18 shows the relation between inlet pressure and MQE of the prototype and EF-L conductor test samples. In the measurement, the mass flow rate is about 4.0 g/s. The characteristics of SHe varies drastically with the pressure change, so that the relation is unknown.

3.4. Measurements of self-magnetic field

Self-magnetic fields of the conductor test samples were measured using Hall sensors to investigate the position of a current center of the samples during the Tcs measurement [17, 18]. Based on the results of the self-magnetic fields, the current centers were analyzed. The current center at normal propagation was calibrated to be positioned at the center of the conductor cross-section because conductor current distribution was assumed to be uniform at the normal propagation. Figs. 19 and 20 show the current centers of the prototype, EF-H, and EF-L samples, respectively. The current center of the EF-H and EF-L samples were stable even if normal propagation occurred. On the other hand, the current center of the prototype sample moved after normal propagation as shown in Fig. 21. The analytical results indicated that the current distributions of the EF-H and EF-L samples are uniform, and that of the prototype sample is non-uniform during Tcs measurements. In section 7.2, a cause of the non-uniform current distribution is discussed.

4. Conductor tests for CS coil

4.1. Conductor test sample

CS coils of the JT-60SA are subjected to a maximum magnetic field of 8.9 T. Therefore, a CIC conductor composed of Nb_3Sn strands was used as a CS conductor. Specifications of the conductor are listed in Table 5. Fig. 22 shows the cross-section of the CS conductor. A cable of the CS conductor consists of 216 Nb_3Sn strands plated with Cr and 108 copper wires. The conductor is equipped with a central spiral made of SS316L, and sub-wrapped tapes are not utilized in the conductor. A conduit of the conductor is composed of SS316LN.

The configuration of a conductor test sample is hairpin shaped, which is composed of one inlet and two outlets for SHe. Figs 23 and 24 show the schematic view and photograph of the sample in which the straight section is 600 mm long. At the straight section, the length of the external field with 95 % uniformity is 200 mm, which is longer than the final twist pitch of the CS conductor. In terms of Tcs measurement, voltage taps and thermometers are mainly attached on the conduit at the straight section. Details of the test conductor sample are described in Refs. [19, 20].

4.2. Measurements of current sharing temperature

Tcs measurement of a CS conductor sample was conducted using the test facility for large superconducting conductors [19]. In this conductor test, the sample was subjected to repeated electromagnetic (EM) cycles and thermal cycle before or after the Tcs measurement. The conditions of EM cycles are as follows: the operating current is 22.6 kA and the magnetic field is 8.0 T. The EM cycle's condition was almost the same as a real operating condition of the CS coil in which the operating current is 20 kA and the magnetic field is 8.9 T. The EM cycles were conducted up to 4000 cycles, and one thermal cycle was conducted after the EM cycles reached 2000. In the Tcs measurement, the

procedure for the CS conductor sample was the same as that for the EF conductor samples. The Tcs criteria was determined to be 10 μV/m.

Fig. 25 shows the Tcs measurement results of the sample at (+) and (-) sides before the repeated EM cycles. The measurement results fulfilled the design requirement, which is 7.08 K at 18.7 kA under the magnetic field of 9 T. The Tcs at (-) side was about 0.2 K higher than that at (+) side. To investigate a cause of the difference between both sides, thermal strain of the sample was measured at room temperature using strain gauges after the completion of the Tcs measurements. As a result, the strain at (+) side was larger than that at (-) side. A cause of the Tcs difference at both sides will be the difference of the thermal strain.

The results of the Tcs measurement subjected to EM cycles and thermal cycle are shown in Fig. 26. In this measurement, Tcs of the sample was measured at 22.6 kA under the magnetic field of 8.0 T including the self-field of 0.3 T, and the design requirement of Tcs was 7.51 K. The measured Tcs was stable and always above the requirement during the cycles. Consequently, the results indicated that there is no degradation of the CS conductor sample due to 4000 EM cycles and one thermal cycle.

5. Joint tests for EF coil

5.1. Joint sample

A shake-hands lap joint was adopted for the EF coils to fabricate a joint at a low cost. In the joint tests, a “prototype joint,” “pancake joint,” “terminal joint,” and “feeder joint” were developed as a joint sample. Figs. 27 and 28 show the schematic view and photograph of the prototype joint sample. The prototype joint sample is a U-shaped configuration which is composed of the prototype conductors removing a jacket [13]. The cross-section of the joint is shown in Fig. 29. A saddle spacer of oxygen-free copper (C1020) was located between the conductors removing Ni plating of NbTi strands. The conductors and spacer were electrically connected with solder (Sn50-Pb50) and clamped with SS316L. In addition, the central spiral was replaced with a SS tube in the joint. The void fraction of the conductors in the joint was 25%, and the connected length was 160 mm.

Figs. 30 and 31 show the schematic view and photograph of the joint sample for the pancake and terminal joints. The sample has a racket shape the circular section of which is 300 mm in diameter [21]. The pancake joint is composed of the shake-hands lap joint between the EF-H conductors, and the terminal joint is composed of the shake-hands lap joint between the EF-H and EF-L conductors. The cross-section of the pancake joint is shown in Fig. 32. The configurations of the pancake and terminal joints are almost the same as the prototype joint, but there are some differences. In the pancake and terminal joints, screws were used with clamps to lock the conductors. In addition, SS304 instead of SS316 for clamps and screws and C1100 instead of C1020 for a saddle spacer were utilized to reduce material cost.

The feeder joint sample has a U-shaped configuration composed of the EF-H and EF-L conductors removing a jacket, as shown in Fig. 27. The cross-section of the feeder joint is the same as that of the terminal joint sample. Fabrication of the feeder joint will be conducted on-site after the EF coils have been assembled to the JT-60SA device. Hence, fabrication method and tools were developed to conduct joint fabrication at a narrow workspace in the vertical direction [22].

5.2. Measurements of joint resistance

Joint resistance of a racket-shaped sample for the pancake and terminal joints was measured using the test facility for large superconducting conductors. The thermal insulation vessel and heat exchanger were removed from the test facility, and the sample was immersed in LHe [21]. Fig. 33 shows the joint resistances of the pancake and terminal joints. In the measurement, the operating current of the sample was 20 kA. The resistances of both joints are proportional to the external field, and the resistance of the pancake joint is slightly lower than that of the terminal joint. The resistances of the pancake and terminal joints are 1.85 nΩ and 2.1 nΩ, respectively, at the external field of 3T. These results fulfilled the design requirement that is 5 nΩ at 3 T.

The joint resistance measurement of U-shaped samples for the prototype and feeder joints were conducted using the test facility for middle-sized superconducting conductors [13, 22]. The measurement results of the samples are shown in Fig. 34. The operating current of both samples was 20 kA. Similar to the pancake and terminal joints, the joint resistance of the prototype and feeder joints are proportional to the external field due to magnetic resistance of a saddle shaped-spacer. The resistance of the feeder joint is 1.68 nΩ at 2 T. This result satisfied the design requirement that is 5 nΩ at 2 T. From the measurement result of each joint sample, the validity of the joint fabrication for the EF coil was confirmed.

5.3. Measurements of self-magnetic field

Self-magnetic field generated by the joint was measured using Hall sensors to evaluate current distribution at the joint. As a joint sample, the prototype and feeder joint samples were used. As shown in Fig. 29, Hall sensors were longitudinally arranged between conductors on the SS plate for the prototype joint sample or clamp for the feeder joint sample. The position of the Hall sensors for the feeder was shifted 5 mm in the x direction from the center axis of the joint cross-section. Figs. 35 and 36 show the measurement and calculation results of the prototype and feeder joint samples, respectively. In the calculation, a line current model assuming uniform current distribution at the joint was used. The details of the model are described in Ref. [13]. The measurement results are in good agreement with the calculation results. As a result, the current distribution of both samples would be uniform at the joint.

6. Joint tests for CS coil

6.1. Joint sample

In the JT-60SA CS coil, there are two joint types “pancake joint” and “terminal joint.” For the configuration of the pancake joint, a butt joint was adopted because the butt joint is suitable for situations where conductors are joined in a narrow space. Hence, the pancake joint can realize embedding of the joint into a winding pack to provide maximum magnetic flux at a given peak field in the winding [1]. For the configuration of the terminal joint, a shake-hands lap joint was adopted to fabricate a joint at a low cost. To evaluate the validity of the joint fabrication for the CS coil, joint samples were developed.

The schematic view and photograph of the butt joint sample are shown in Figs. 37 and 38. The sample is hairpin-shaped and consists of two butt joints using the JT-60SA CS coil conductors [23, 24]. The sample has a single

inlet and double outlets for SHe. A case made of SS316 is used to make the sample hairpin curve instead of the conduit. At the termination, Nb_3Sn cables are connected to an oxygen-free copper plate by sinter bonding.

Fig. 39 shows the configuration and photograph of the butt joint without the conduit. The cross-section of the butt joint with the conduit is shown in Fig. 40. In butt joint fabrication, the conduit is removed to expose the Nb_3Sn cable before heat treatment of the Nb_3Sn strands. The central spiral is replaced with a cone-shaped flow distributor. The cables are compacted to 2% void fraction using copper sleeves. After the heat treatment, joining surfaces of the cables are cut and polished. Subsequently, a 0.1-mm-thick copper sheet is inserted in the surfaces. The joining part is heated for diffusion bonding in a vacuum. The conduit and spacers are then assembled. The joint fabrication of the butt joint is described in Ref. [25].

For the terminal joint, two samples based on the shake-hands lap joint, which are "Type A" and "Type B," were developed [26]. The schematic view and photograph of the joint sample are shown in Figs. 41 and 42. The joint sample is hairpin-shaped and composed of one joint using the CS and EF-L coil conductors. Fig. 43 shows the fabrication process of both joints. In the Type A, a Nb_3Sn cable is inserted into a copper pipe and the pipe is swaged. Then the heat treatment of the Nb_3Sn cable is conducted, and the cable is sintered to the pipe during the heat treatment. Subsequently, a copper spacer and the copper pipe are joined with a high temperature solder (S50), and a NbTi cable and the spacer are joined with a solder (H60A).

In Type B, a Nb_3Sn cable and copper spacer are directly joined without the copper pipe. The Nb_3Sn cable is heat-treated while pressing the cable to the spacer, and the cable and spacer are joined through sintering. Then, a NbTi cable and the spacer are joined with a solder (H60A). Details of the joint fabrication for the terminal joint are described in Ref. [26].

6.2. Measurements of joint resistance

Joint resistances of the pancake joint sample were measured using the test facility for large superconducting conductors. The sample was cooled by supplying SHe into a cooling channel of the sample. For the measurement, SHe temperature was controlled using a film heater and a thermometer attached to the inlet pipe. Fig. 44 shows the measurement results of joint resistance. The measurements indicated that the performance of the pancake joint fulfilled the design requirement in which the joint resistance was less than 5 nΩ at 2 T [23].

The joint resistance measurements of the terminal joint samples were conducted at the test facility for large superconducting conductors. During the measurement, the samples were cooled by immersing the sample in LHe. Fig. 45 shows the measurement results of the samples. The joint resistance of the Type A joint sample was 1.2 nΩ under the external field of 4 T, which fulfilled the design requirement, which was 5 nΩ. On the other hand, the joint resistance of the Type B joint sample was 16.8 nΩ even without the external field [26]. Consequently, the Type A joint was adopted as the CS terminal joint.

The Type B joint sample was disassembled to investigate a cause of high joint resistance of the sample. As a result, the contact between a Nb_3Sn cable and copper spacer was poor because the configuration of the copper spacer was deformed owing to creep phenomenon during heat treatment [26].

6.3. Quench tests

For the pancake joint sample, quench tests were conducted to investigate stable operating conditions of the butt joint [23, 24]. In the tests, the quench current was measured under several conditions. Fig. 46 shows the result of quench current under each external field at the mass flow rate of 3 g/s. The quench current of the pancake joint can be increased by decreasing external field and/or operating temperature. The real operating condition of the butt joint is 20 kA at 7 K under 2 T. Hence, the pancake joint has a temperature margin of 4 K for real operating temperature.

7. Discussion

7.1. Potential of the NIFS test facility

As described in section 2, the test facility for large superconducting conductors was specialized for pool-cooled conductors before. For the JT-60SA conductor and joint tests, the test facility was modified adding SHe cooling system. The modified test facility was able to realize the various test conditions for CIC conductor and joint samples. In addition, the test results of the conductor and joint samples fulfilled the design requirements. Through the success of the JT-60 SA conductor and joint tests, the validity of the NIFS test facility was fully confirmed as a test facility for CIC conductors. Consequently, the joint tests of the ITER TF have been conducted using the NIFS test facility since 2013 [27]. In the future, we expect to use the NIFS test facility for the developments of conductor and joint aiming to the DEMO nuclear fusion power plant, provided that the required magnetic field strength is within 9 T. Additionally, at present, we are constructing a new test facility which can generate a high magnetic field up to 13 T using a superconducting solenoid coil, the bore of which is 0.7 m [28]. Using the new test facility, the conductor development for the DEMO will be accelerated.

7.2. The effect of sub-wrapping tapes on conductor performance under DC operation

As described in section 3.4, during Tcs measurements of the EF coil conductors, the current centers of the EF-H and EF-L conductors were stable, as shown in Figs. 19 and 20. On the other hand, the current center of the prototype conductor was changed before-and-after normal propagation occurred, as shown in Fig. 21. These results indicated that the current distributions of the EF-H and EF-L conductors are uniform, and that of the prototype is not uniform during the Tcs measurement. The cause of the non-uniform current distribution is attributed to the sub-wrapping tapes used for the prototype sample. The sub-wrapping tape can prevent current transfer between strand bundles, so that the tapes are useful to reduce coupling loss generated by changing conductor current. In DC operation of the conductor, however, the tapes tend to hamper current redistribution among strand bundles.

As described in section 3.3, the stability of the prototype conductor at 30 kA was not improved with the increase of the temperature margin, compared to other operating conditions, as shown in Fig. 16. The inductive heater can apply heat uniformly to each sub-cable covered with sub-wrapping tapes. Hence, the current distribution of the prototype at 30 kA would be unbalanced, similar to the Tcs measurement.

From the conductor test results, the sub-wrapping tapes may deteriorate the conductor performance under DC operation. Therefore, the sub-wrapping tapes are not necessary for CIC conductors used in toroidal field coils for tokamak machines and helical coils for stellarator machines which are operated in DC. In addition, by adjusting either the void fraction of the conductor or the thickness of strand plating, the CIC conductor without the sub-wrapping tapes can be used in CS and EF coils which require rapid change of operating current.

7.3. Stable performance of CS conductor sample subjected to EM load cycles

In the Tcs measurements of the CS conductor sample, the performance of the sample was stable even though the sample was subjected to repeated EM load cycles and thermal cycle, as shown in Fig. 26. On the other hand, several test results of the ITER TF and CS conductor samples, which are composed of Nb_3Sn strands, demonstrated that the conductor performance is degraded by repeated EM cycles and thermal cycles [29]. To clarify the reason why the JT-60SA CS conductor sample was not degraded in the conductor test, the details of the ITER CS conductor tests were investigated with references [29, 30].

The ITER CS conductor tests have been conducted using the SULTAN facility composed of superconducting split coils, which can generate a magnetic field up to 10.85 T [31, 32]. The length of a high field region is about 400 mm. The conductor sample used in the SULTAN facility is composed of two straight conductors jointed at the top and bottom, and the sample length is 3.6 m. The conductor sample is excited using a superconducting transformer. Specifications of the ITER CS conductor are listed in Table 6. Compared to the JT-60SA CS conductor, the ITER CS conductor has a capability of dealing with a larger current and stronger magnetic force.

Although there are some slight differences in sample configuration, an external field distribution, and other features, the conductor tests of the JT-60SA CS and ITER CS have in common, in terms of testing of short straight CIC conductors under static magnetic field generated by split coils. Details of the test conditions for the JT-60SA CS and ITER CS conductor samples are listed in Table 7. In the test of the ITER CS, the sample was subjected to three types of EM load. According to the reference [29], the conductor performance of the ITER CS conductor is degraded by the EM load cycles more than 416 kN/m. On the contrary, the conductor performance subjected to the EM load cycles less than 343 kN/m was nearly-constant. From these results, Nabara suggests that a fatigue limit may exit on a CIC conductor.

EM stress, which is EM load divided by half of the circumference of a jacket inner, was used as an index parameter to compare the JT-60SA CS with the ITER CS in terms of EM loads for conductor sample. As listed in Table 7, the EM stress of the JT-60SA CS is lower than the smallest EM stress that is unable to degrade the ITER CS conductor. Hence, the EM load for the JT-60SA CS conductor was so low that the conductor performance was stable during the test.

7.4. Evaluation of conductor joint using self-field measurements

Superconducting fusion magnets are composed of many conductor joints which have a great impact on the performance of the magnets. Hence, the conductor joints must be evaluated precisely. As an evaluation method of the conductor joints, joint resistance and AC loss measurements [33, 34] are standard at present. Although the necessity of these measurements are well-known, these measurements are not sufficient because the current distribution at the conductor joint, which can indicate the joint condition, are unknown. To realize a more precise evaluation of the conductor joint, we propose self-field measurement at the conductor joint. As described in section 5.3, the self-field measurement results can reveal the current distribution at the conductor joint using an analytical model. With regards to the preparation of the self-field measurement, Hall sensors are only mounted at the conductor joint. The self-field measurement can be conducted together with the joint resistance measurement, so that the self-field measurement is a simple solution to implement as a new standard for joint evaluation.

8. Conclusion

The collaborative project between JAEA and NIFS was launched to evaluate the performance of the CIC conductors and conductor joints for the JT-60SA CS and EF coils using the NIFS test facility in 2007. Conductor tests for four types of CIC conductors and joint tests for seven types of conductor joints have been conducted for the past eight years. As a result, we confirmed that the CIC conductors and conductor joints fulfill the design requirements. From the achievements of this project, we expect to use the NIFS test facility for the development of conductor and conductor joint, aiming for the DEMO nuclear fusion power plant, provided that the required magnetic field strength is within 9 T.

Acknowledgments

The authors wish to thank Mr. K. Ueda, Mr. J. Fukuhara, and Mr. K. Tamada of Taiyo Nippon Sanso Co. Ltd. and the operating staffs of Hitachi Co. Ltd. for the cooling system operation of the test facility. The authors also wish to thank Mr. Sugito, Mr. Okada, Dr. Tamura, Dr. Yanagi, and Dr. Takada of NIFS and Mr. Terazaki of SOKENDAI, and Mr. Yamamoto of Sophia University for their technical support.

References

[1] K. Yoshida, K. Tsuchiya, K. Kizu, H. Murakami, K. Kamiya, T. Obana, et al., Development of JT-60SA superconducting magnet system, Physica C, 470 (2010) 1727-1733.
[2] H. Murakami, K. Kizu, K. Tsuchiya, Y. Koide, K. Yoshida, T. Obana, et al., Development and Test of JT-60SA Central Solenoid Model coil, IEEE Transactions on Applied Superconductivity, 24 (3) (2014) 4200205.
[3] Y. Kamada, P. Barabaschi, S. Ishida, the JT-60SA Team and JT-60SA Research Plan Contributors, Progress of the JT-60SA Project, Nuclear Fusion, 53(2013) 104010.
[4] K. Yoshida, H. Murakami, K. Kizu, K. Tsuchiya, K. Kamiya, Y. Koide, et al., "Mass Production of Superconducting Magnet Components for JT-60SA", IEEE Trans. Appl. Supercond., 24(2014) 4200806.
[5] K. Kizu, K. Tsuchiya, T. Obana, K. Takahata, R. Hoshi, S. Hamaguchi, et al., Critical current measurement of prototype NbTi cable-in-conduit conductor for JT-60SA, Fusion Engineering and Design, 84 (2009) 1058-1062.
[6] T. Obana, K. Takahata, S. Hamaguch, N. Yanagi, T. Mito, S. Imagawa, et al., Upgrading the NIFS superconductor test facility for JT-60SA cable-in-conduit conductors, Fusion Engineering and Design, 84 (2009) 1442-1445.
[7] N. Yanagi, T. Mito, S. Imagawa, K. Takahata, T. Satow, J. Yamamoto, et al., Development and quality control of the superconductors for the helical coils of LHD, Fusion Eng. Des. 41 (1998) 241–246.
[8] K. Takahata, T. Mito, T. Satow, N. Yanagi, M. Sakamoto, S. Yamada, et al., Stability of cable-in-conduit superconductors for Large Helical Device, IEEE Transactions on Applied Superconductivity, Vol. 3, No. 1 (1993) 511-514.
[9] J. Yamamoto, T. Mito, K. Takahata, S. Yamada, I. Ohtake, A. Nishimura et al., Superconducting test facility of NIFS for the Large Helical Device, Fusion Eng. Des. 20 (1993) 147–151.

[10] J. Yamamoto, T. Mito, K. Takahata, N. Yanagi, S. Yamada, I. Ohtake, A cryogenic system for the superconducting magnet testing facility, Advances in Cryogenic Engeering, Vol. 37, Plenum Press, New York, 1992, pp. 755-762.
[11] S. Yamada, T. Mito, S. Tanahashi, H. Kubo, Y. Yonenage, R.Watanabe, et al., Characteristics of a dc 75 kA power supply in the superconducting magnet test facilities, Fusion Eng. Des. 20 (1993) 201–209.
[12] T. Mito, K. Takahata, N. Yanagi, S. Yamada, A. Nishimura, M. Sakamoto, et al., Development of 100 kA current leads for superconductor critical current measurement, Fusion Eng. Des. 20 (1993) 217–222.
[13] T. Obana, K. Tahakata, T. Mito, S. Imagawa, K. Kizu, H. Murakami, K. Yoshida, Magnetic Field Measurements on a Shake-Hands Lap Joint Sample of Cable-In-Conduit Conductors for JT-60SA EF Coil, IEEE Transactions on Applied Superconductivity, Vol. 20, No. 3 (2010) 1471-1474.
[14] K. Kizu, Y. Kashiwa, H. Murakami, T. Obana, T. Takahata, K. Tsuchiya, et al.,Fabrication and tests of EF conductors for JT-60SA, Fusion Eng. Des. 86 (2011) 1432–1435.
.[15] H. Murakami, T. Ichige, K. Kizu, K.Tuchiya, K. Yoshida, T. Obana, et al., Stability and Quench Test for NbTi CIC Conductor of JT-60SA Equilibrium Field Coil, IEEE Transactions on Applied Superconductivity, Vol. 20, No. 3 (2010) 512-516.
[16] H. Murakami, T. Ichige, K. Kizu, K.Tuchiya, K. Yoshida, T. Obana, et al., Stability Margin of NbTi CIC Conductor for JT-60SA Equilibrium Field Coil, IEEE Transactions on Applied Superconductivity, Vol. 21, No. 3 (2011) 1991-1994.
[17] T. Obana, K. Tahakata, S. Hamaguchi, S. Imagawa, T. Mito, K. Kizu, et al., Study on the dynamic behavior of a current in cable-in-conduit conductors by using self magnetic field measurements, Fusion Eng. Des. 86 (2011) 1377–1380.
[18] T. Obana, K. Tahakata, S. Hamaguchi, H. Chikaraishi, S. Imagawa, T. Mito, et al., Self Magnetic Field Measurements on Cable-In-Conduit Conductors for JT-60SA EF-H and EF-L coils, , IEEE Transactions on Applied Superconductivity, Vol. 22, No. 3 (2012) 4803404.
[19] H. Murakami, K. Kizu, T. Ichige, K. Kamiya, K. Tsuchiya, K. Yoshida, et al., Current sharing temperature of central solenoid conductor for JT-60SA under repetition excitation, Proceedings of ICEC24-ICMC2012, (2013) 575-578.
[20] T. Obana, G. Rolando, E.P.A. Van Lanen, A. Nijhuis, K. Takahata, K. Kizu, et al., Numerical analysis of the DC performance of JT-60SA CS conductor sample, Proceedings of ICEC24-ICMC2012, (2013) 579-582.
[21] T. Obana, K. Tahakata, S. Hamaguchi, T. Mito, S. Imagawa, K. Kizu, et al., Joint resistance measurements of pancake and terminal joints for JT-60SA EF coils, Fusion Eng. Des. 88 (2013) 2773–2776.
[22] K. Kizu, H. Murakami, K. Natsume, K. Tsuchiya, Y. Koide, K. Yoshida, et al., Manufacturing design and development of the current feeders and coil terminal boxes for JT-60SA, Fusion Eng. Des. (2015) to be published.
[23] T. Obana, K. Takahata, S. Hamaguchi, K. Natsume, S. Imagawa, T. Mito, et al., Modeling of Butt Joint Composed of Nb_3Sn Cable-In-Conduit Conductors, Plasma and Fusion Research, Vol. 9 (2014) 3405122
[24] T. Takao, Y. Kawahara, K. Nakamura, Y. Yamamoto, T. Yagai, H. Murakami, et al., Thermal Stability of Butt Joint for CS Conductor in JT-60SA, IEEE Transactions on Applied Superconductivity, Vol. 24, No. 3 (2014) 4800804.
[25] K. Kizu, H. Murakami, K. Tsuchiya, K. Kiyoshi, K. Nomoto, Y. Imai, et al., Development of Central Solenoid for JT-60SA, IEEE Transactions on Applied Superconductivity, Vol. 23, No. 3 (2013) 4200104.
[26] H. Murakami, K. Kizu, T. Ichige, M. Furukawa, K. Natsume, K. Tsuchiya, et al., Development of terminal joint and lead extension for JT-60SA Central Solenoid, IEEE Transactions on Applied Superconductivity, Vol. 25, No. 3 (2015) 4201305.
[27] H. Kajitani,T. Hemmi, T. Mizutani, K. Matsui, M. Yamane, T. Obana et al., Evaluation of ITER TF Coil Joint

Performance, IEEE Trans. Appl. Superconduct. 25(3)(2015) 4202204.
[28] S. Imagawa, T. Obana, S. Takada, S. Hamaguchi, H. Chikaraishi, N. Yanagi et al., Plan for Testing High-Current Superconductors for Fusion Reactors with a 15T Test facility, Plasma and Fusion Research, Vol. 10(2015)3405012.
[29] Y Nabara, T Hemmi, H Kajitani, H Ozeki, M. Iguchi, Y. Nunoya, et al., Examination of Nb3Sn Conductors for ITER Central Solenoids, IEEE Trans. Appl. Superconduct. 23(3)(2013) 4801604.
[30] A. Devred, I. Backbier, D. Bessette, G. Bevillard, M. Gardner, et al., Challenges and status of ITER conductor production, Supercond. Sci. Technol. 27(2014) 044001.
[31] T. Hemmi, Y. Nunoya, Y. Nabara, M. Yoshikawa, K. Mitsui, H. Kajitani, et al., Test results and investigation of Tcs degradation in Japanese ITER CS conductor samples, IEEE Trans. Appl. Superconduct. 22(3)(2012) 4803305.
[32] P. Bruzzone, A. Anghel, A. Fuchs, G. Pasztor, B. Stepanov, M. Vogel, et al., Upgrade of operating range for SULTAN test facility, IEEE Trans. Appl. Superconduct. 12(1)(2002) 520-523.
[33] T. Takao, K. Nakamura, T. Takagi, N. Tanoue, H. Murakami, K. Yoshida, Influence of external magnetic field on AC losses at EF coils joints of JT-60SA, IEEE Trans. Appl. Superconduct. 22(3)(2012) 4704604.
[34] K. Nakamura, Y. Yamamoto, K. Suzuki, T. Takao, H. Murakami, K. Natsume, et al., Evaluation of temperature rise caused by AC loss due to plasma disruption in joint of JT-60SA poloidal field coil, IEEE Trans. Appl. Superconduct. 25(3)(2015) 4200704.

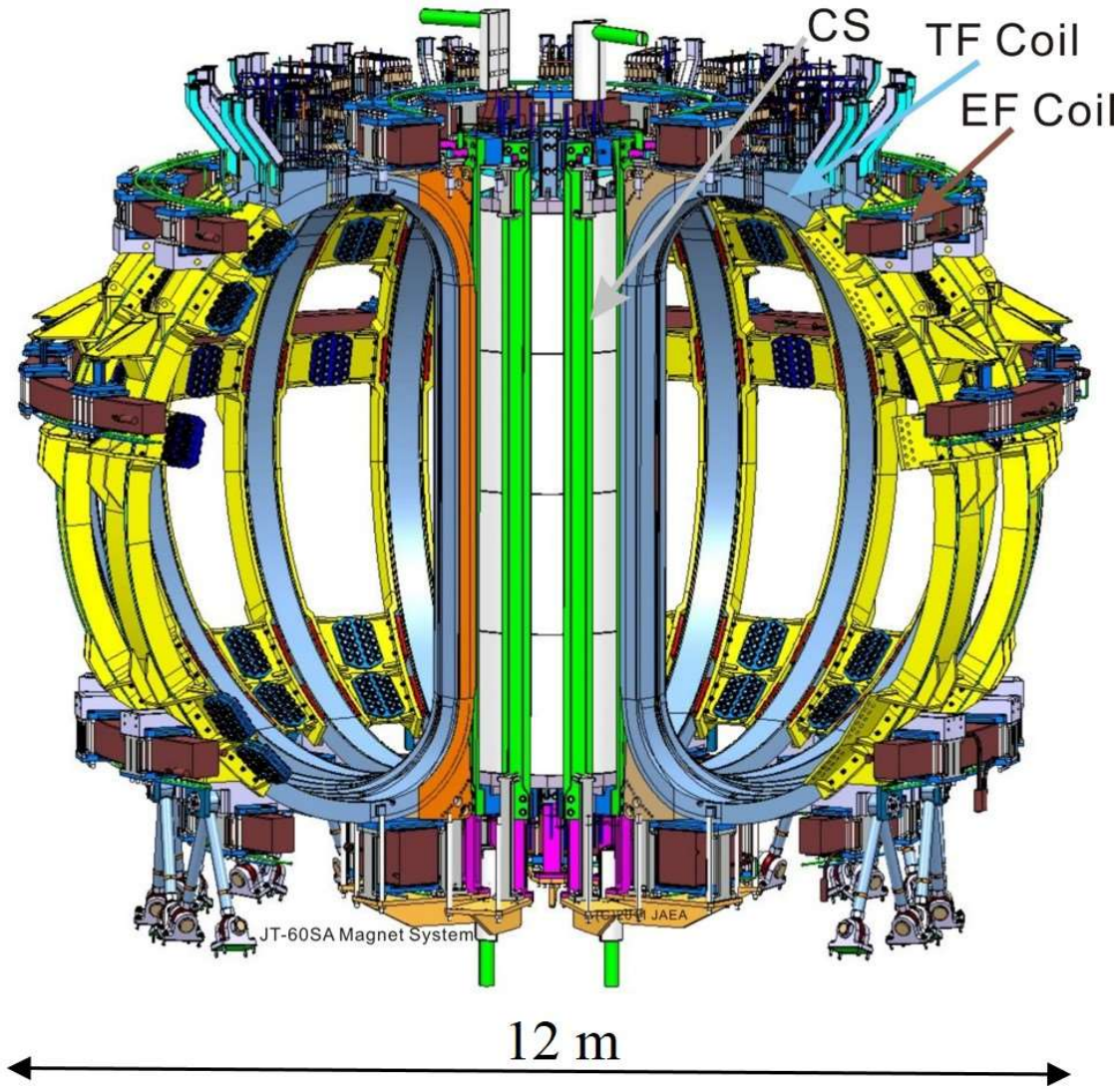

Fig. 1 Schematic view of the JT-60SA magnet system.

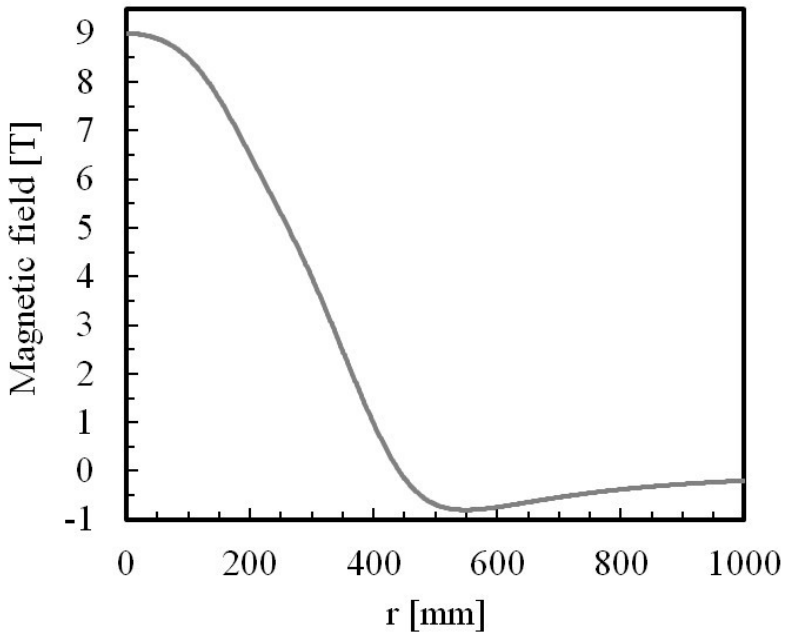

Fig. 2 Magnetic field distribution of the split coil in the test facility for large superconductors. Sign r is the radial distance from the center of the split coil in the test facility.

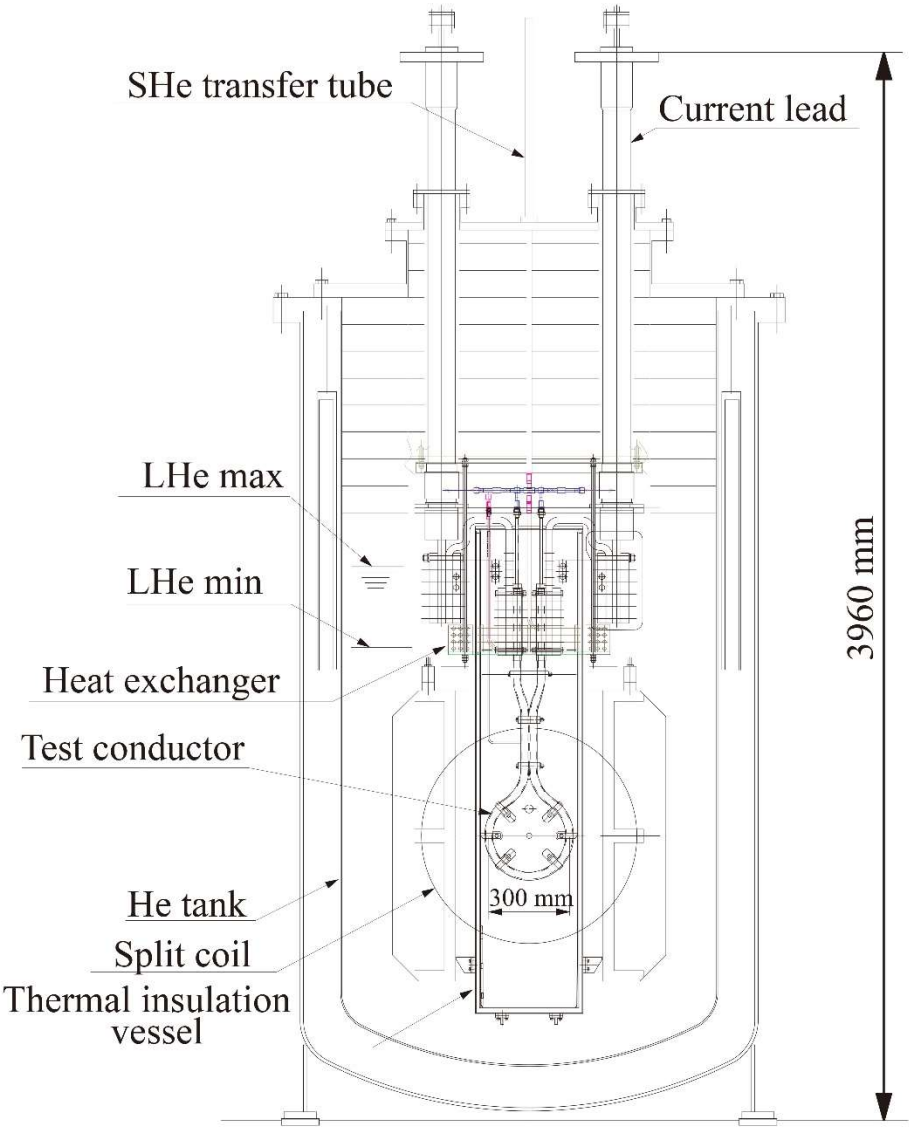

Fig. 3 Schematic view of the test facility for large superconductors.

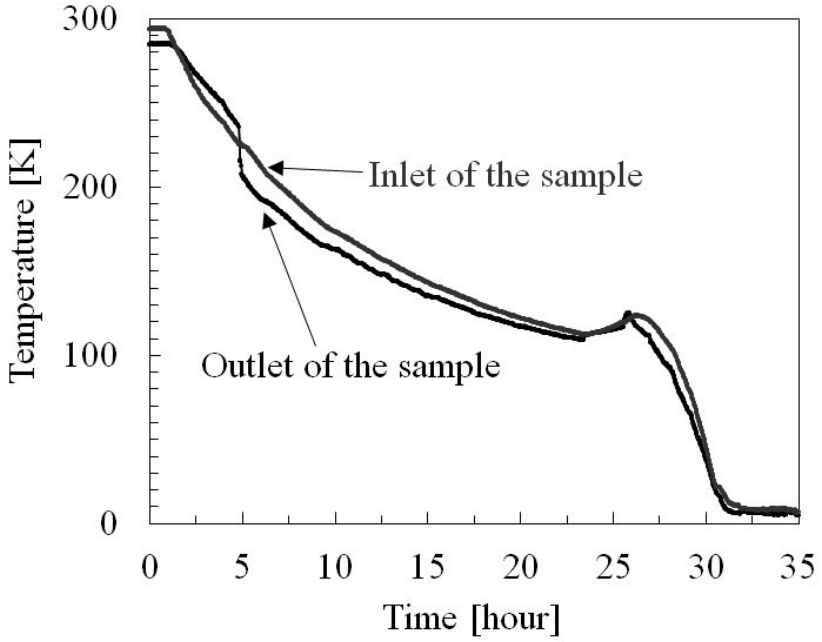

Fig. 4 Cooling curves of a CIC conductor sample in the test facility for large superconductors.

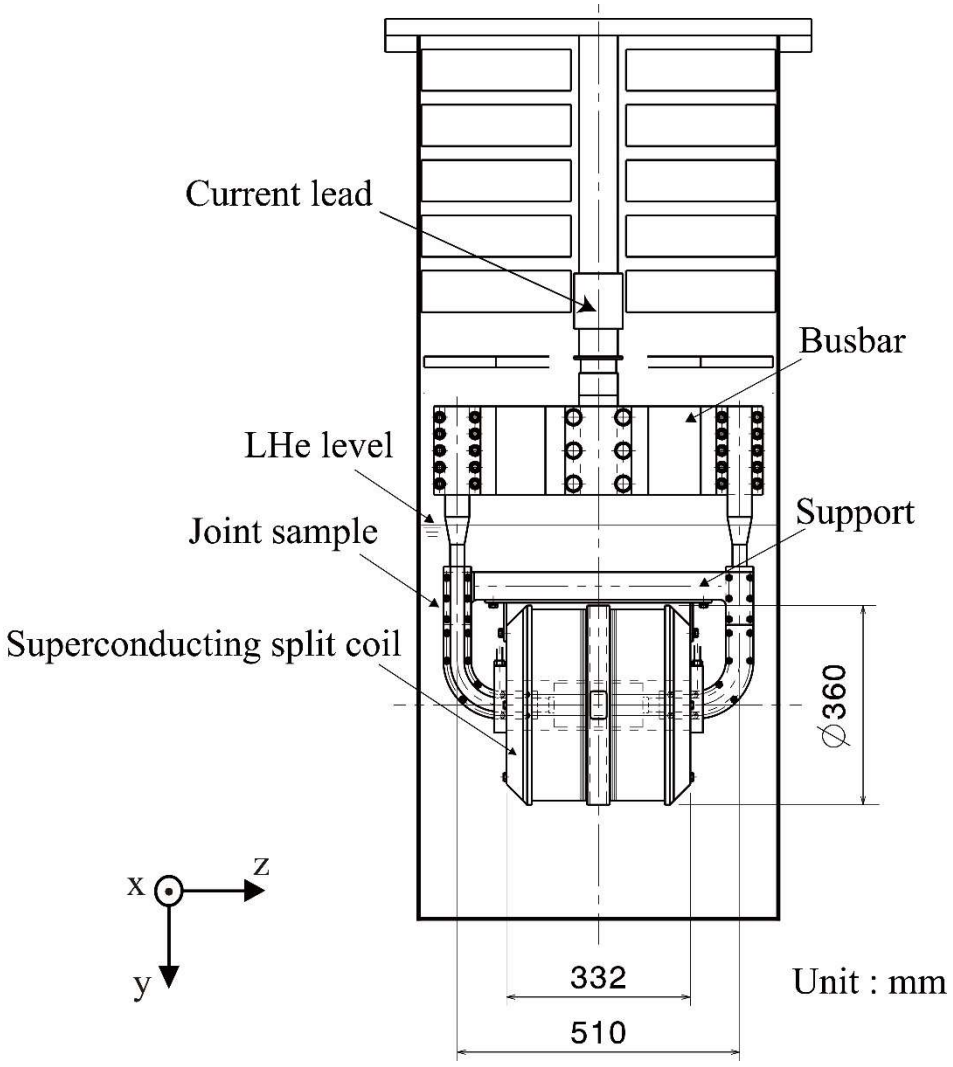

Fig. 5 Schematic view of the test facility for middle-sized superconductors.

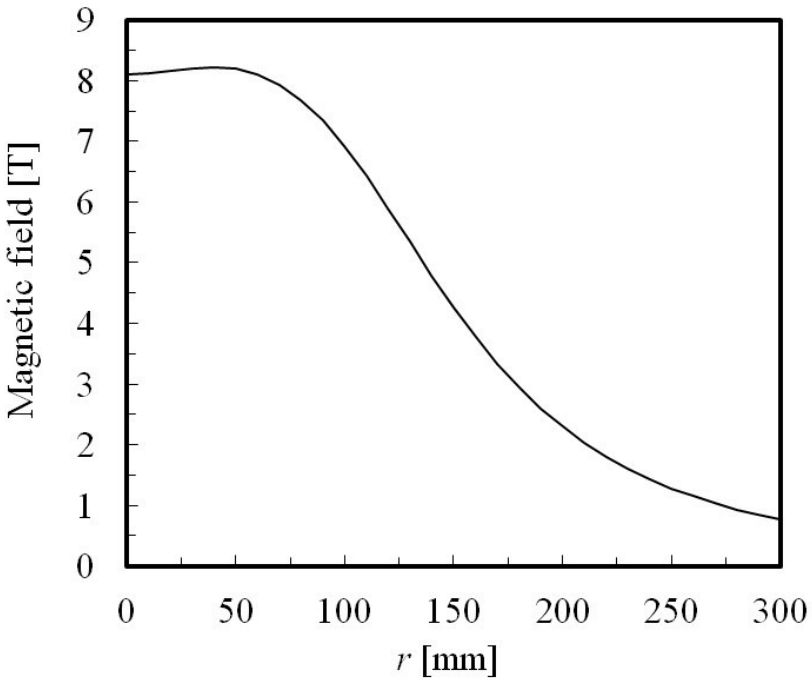

Fig. 6 Magnetic field distribution of the split coil in the test facility for middle-sized superconductors. Sign r is the radial distance from the center of the split coil in the test facility.

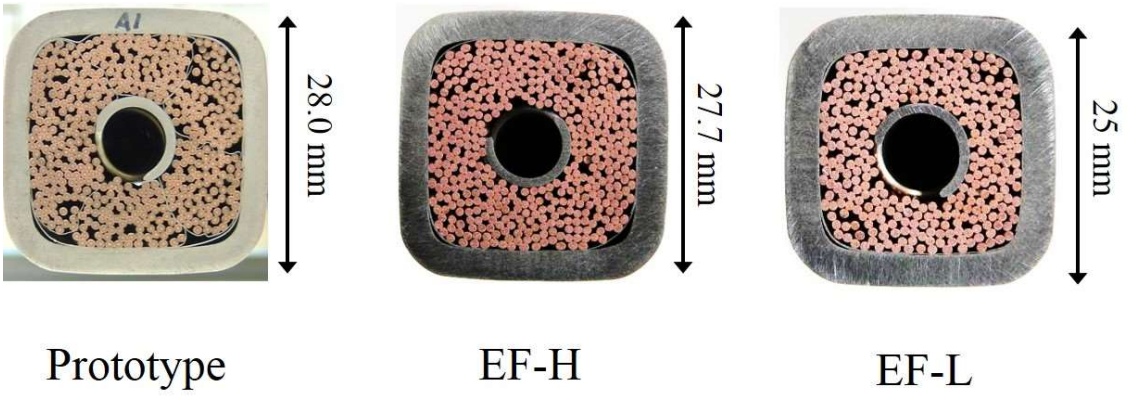

Fig. 7 Cross-sections of the EF coil conductors.

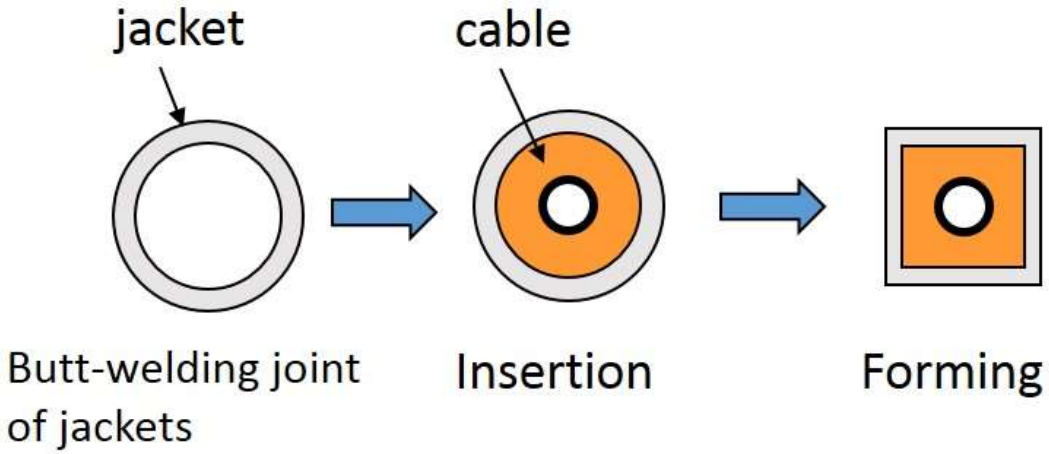

Fig. 8 Fabrication process of the EF coil conductor.

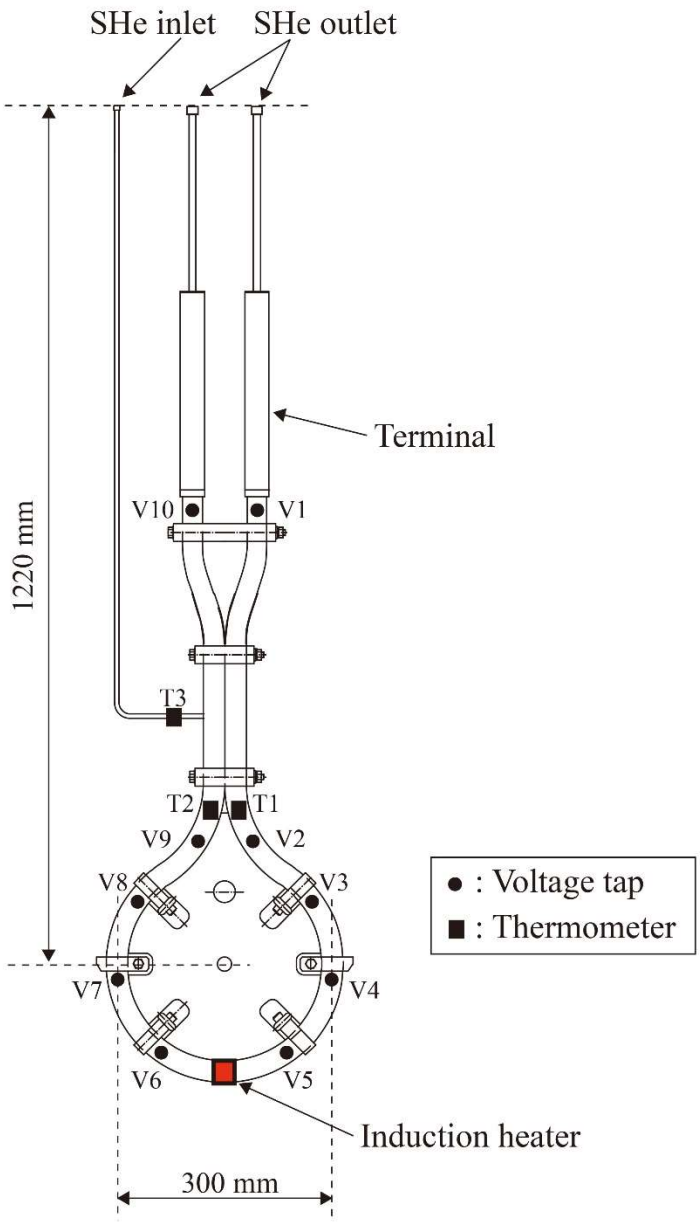

Fig. 9 Schematic view of the conductor sample for the EF coil.

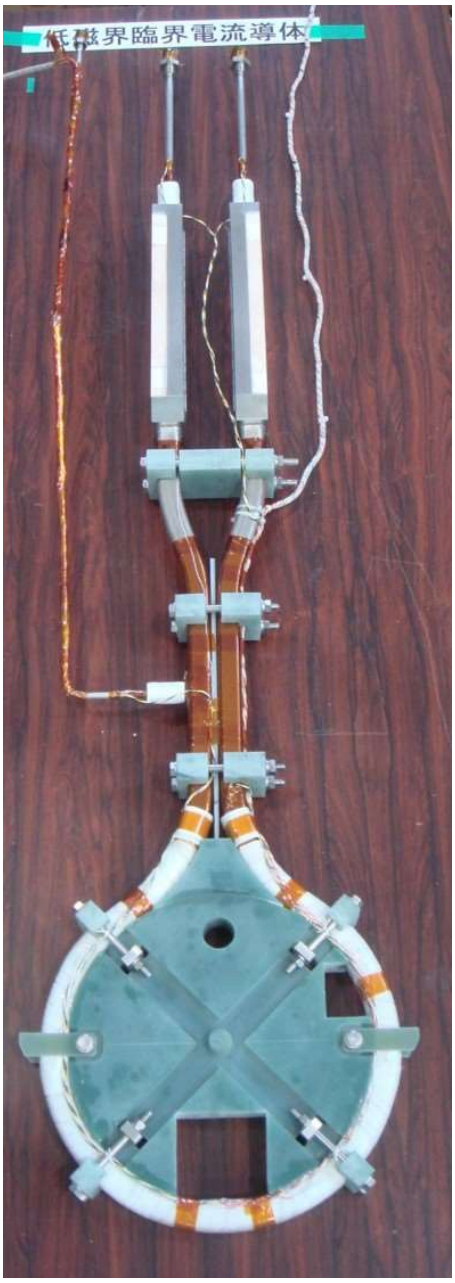

Fig. 10 Photograph of the conductor sample for the EF coil.

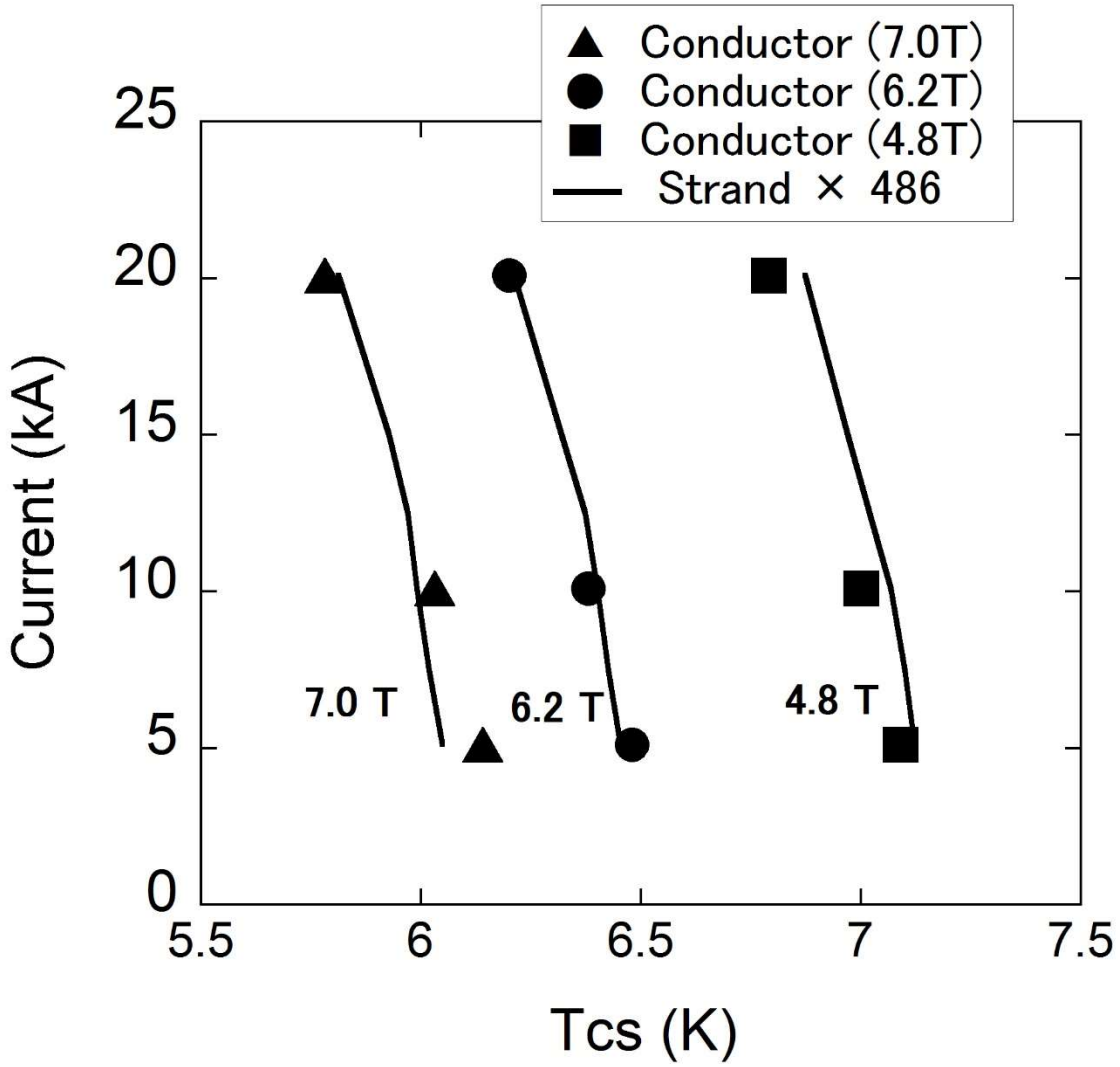

Fig. 11 Tcs measurement results of the prototype conductor sample. The solid line shows the predictive values from NbTi strand critical current.

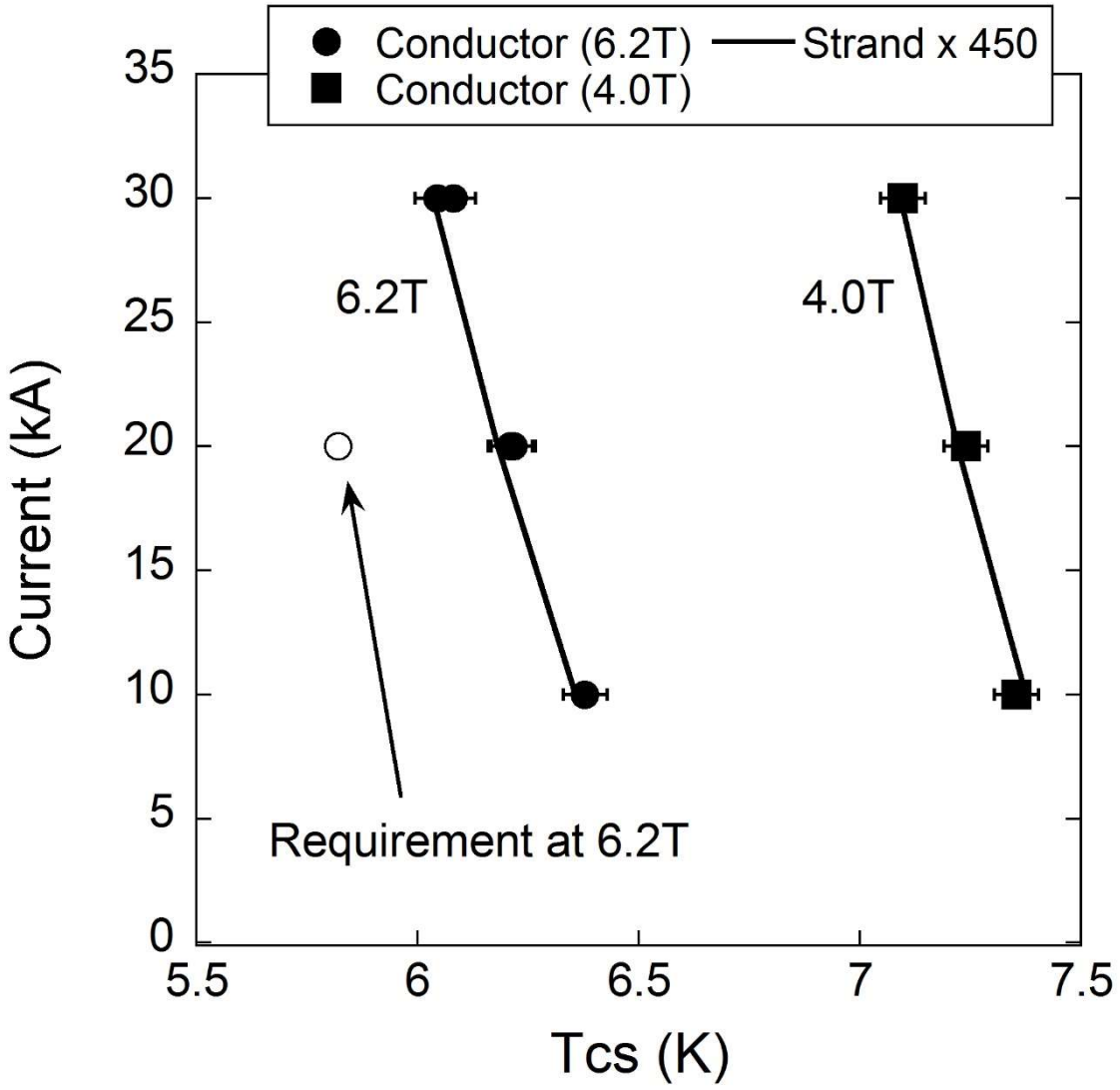

Fig. 12 Tcs measurement results of the EF-H conductor sample. The solid line shows the predictive values from NbTi strand critical current.

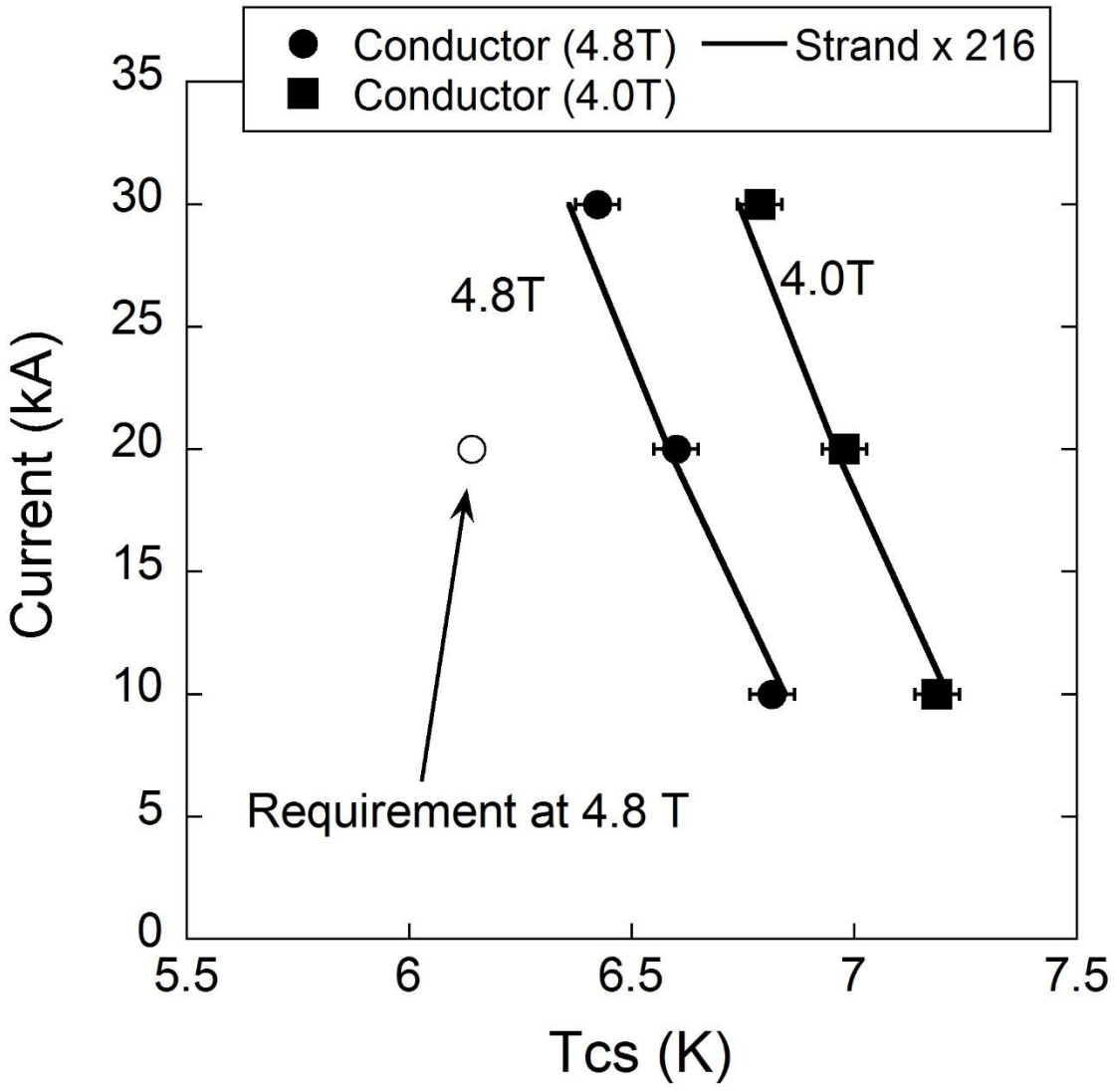

Fig. 13 Tcs measurement results of the EF-L conductor sample. The solid line shows the predictive values from NbTi strand critical current.

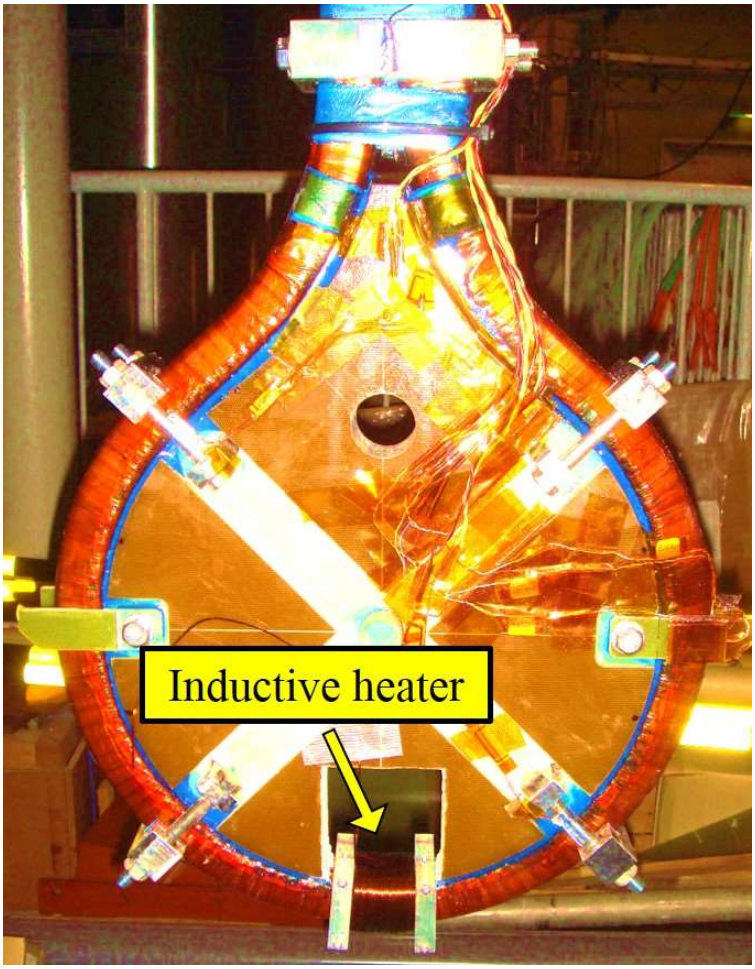

Fig.14 Photograph of the inductive heater mounted on the conductor sample.

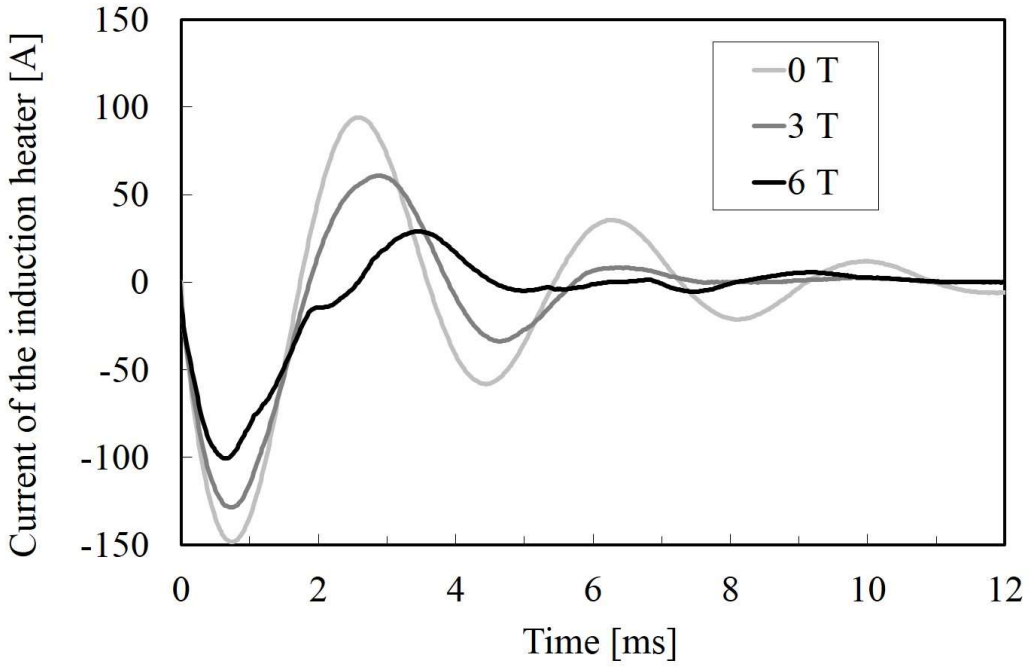

Fig. 15 Current waveforms of the induction heater under several magnetic fields.

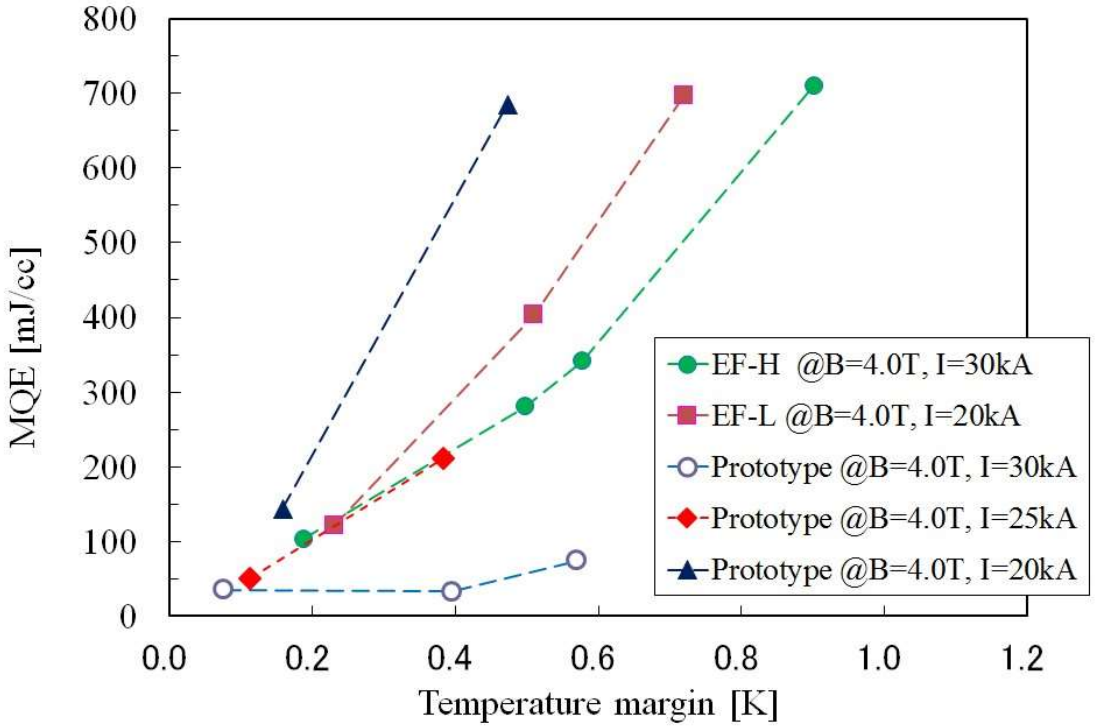

Fig. 16 Stability test results of the EF conductor sample for each temperature margin.
(Temperature margin = current sharing temperature (Tcs) − operating temperature)

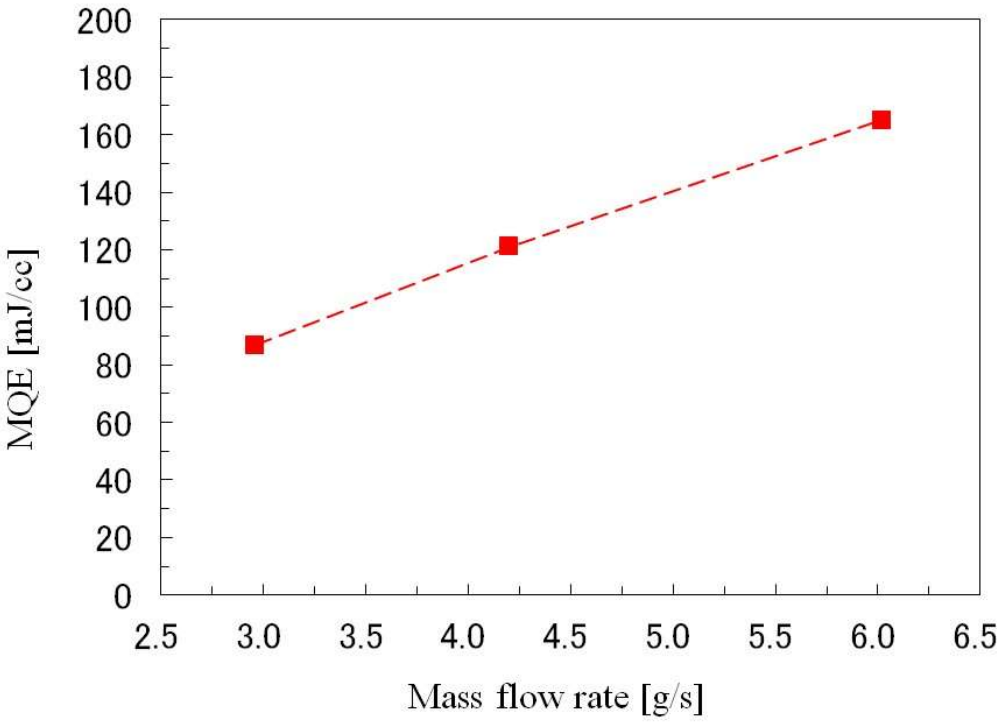

Fig. 17 Stability test results of the EF-L conductor sample for each mass flow rate.

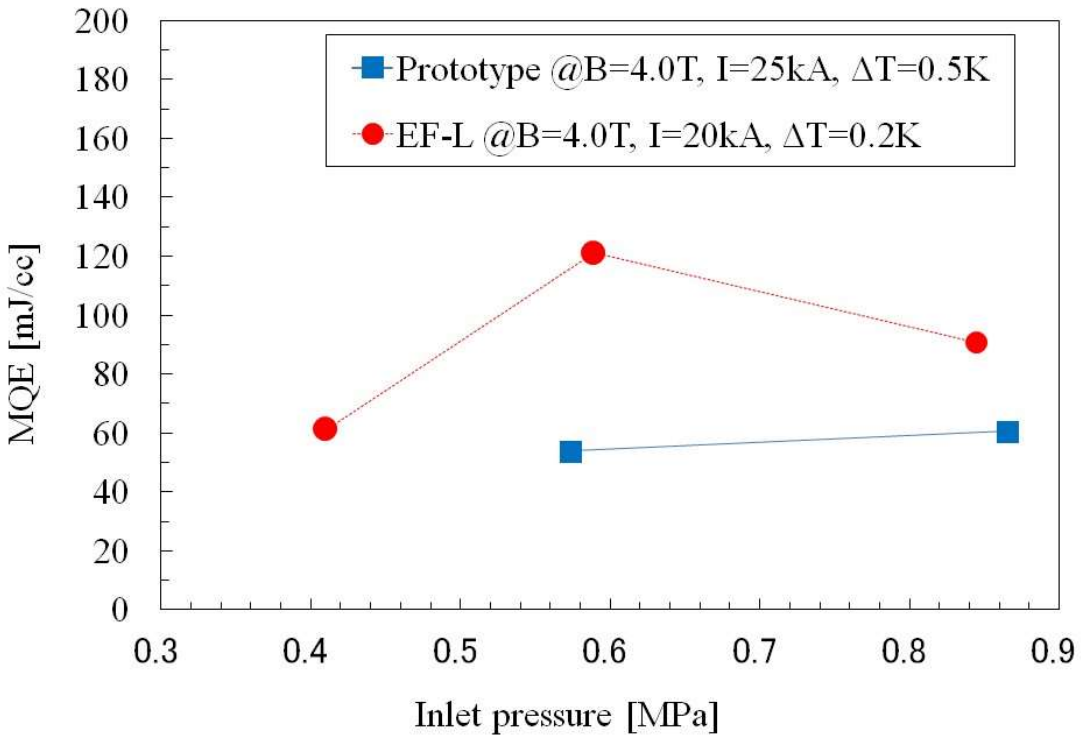

Fig. 18 Stability test results of the prototype and EF-L conductor samples for each inlet pressure.

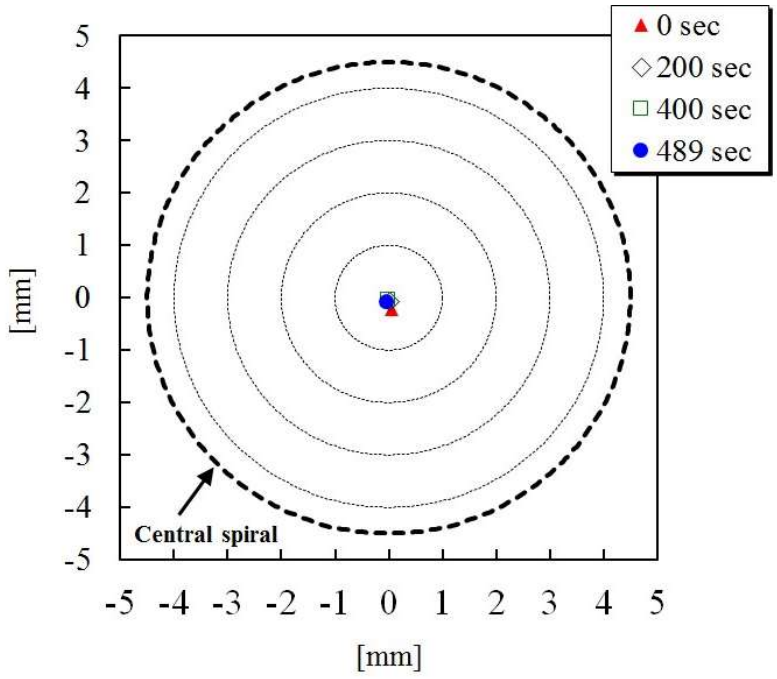

Fig. 19 The position of current center in the cross-section of the EF-H conductor sample during the Tcs measurement. Signs △, ◇, and □ show the position of the current center at 0 sec, 200 sec, and 400 sec. Sign ● shows the position of the current center at 489 sec when the normal propagation occurred.

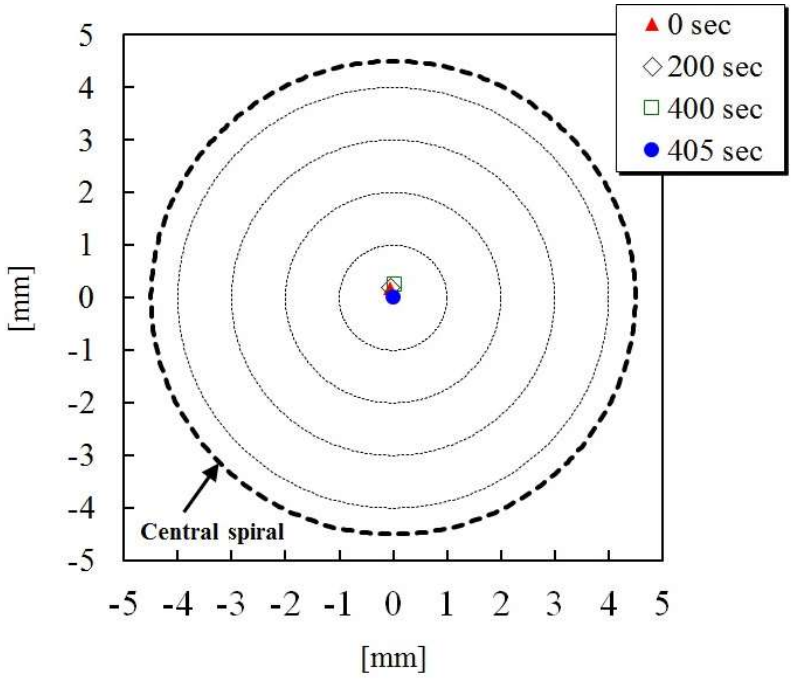

Fig. 20 The position of current center in the cross-section of the EF-L conductor sample during the Tcs measurement. Signs △, ◇, and □ show the position of the current center at 0 sec, 200 sec, and 400 sec. Sign ● shows the position of the current center at 405 sec when the normal propagation occurred.

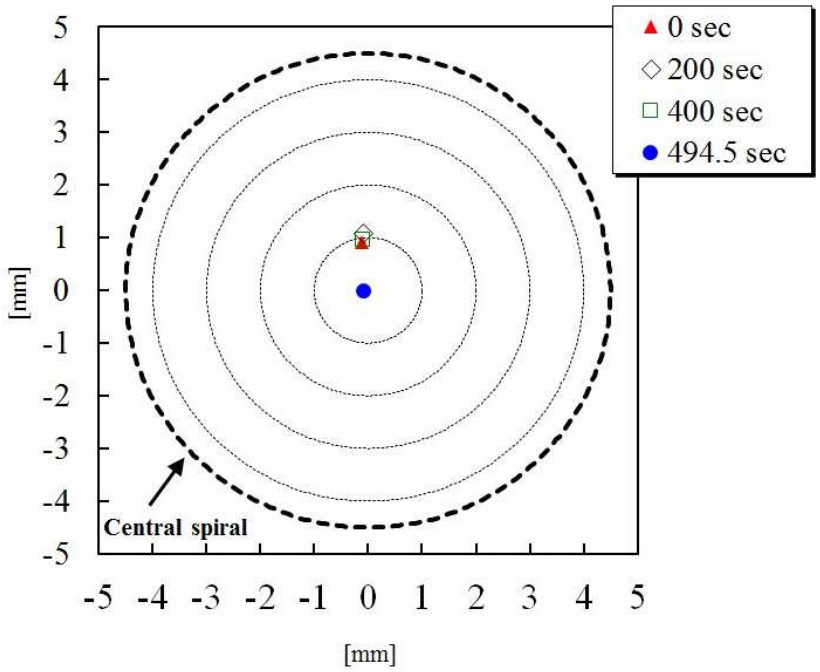

Fig. 21 The position of current center in the cross-section of the prototype conductor sample during the Tcs measurement. Signs △, ◇, and □ show the position of the current center at 0 sec, 200 sec, and 400 sec. Sign ● shows the position of the current center at 494.5 sec when the normal propagation occurred.

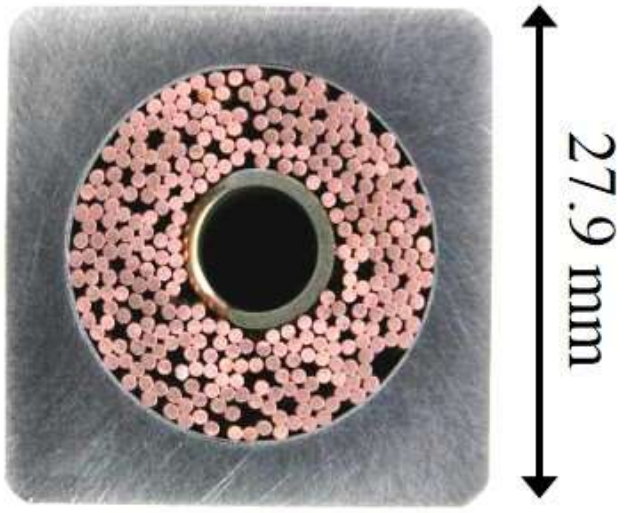

Fig. 22 Cross-section of the CS conductor.

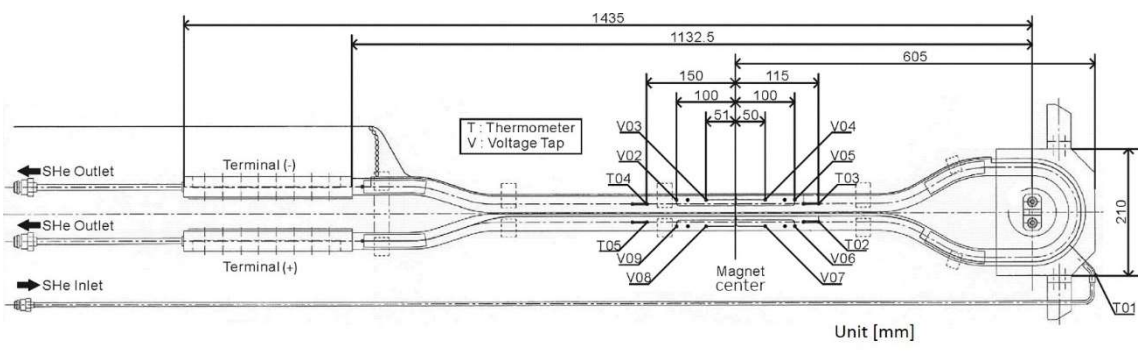

Fig. 23 Schematic view of the CS conductor sample.

Fig. 24 Photograph of the CS conductor sample.

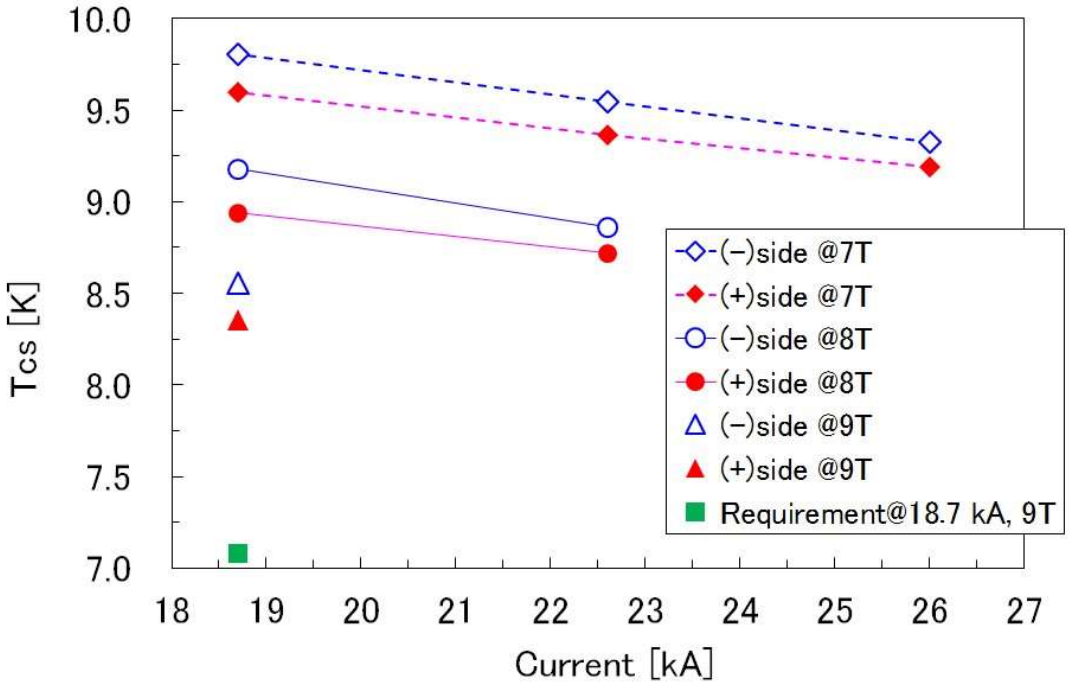

Fig. 25 Tcs measurement results of the CS conductor sample before the repeated EM cycles.

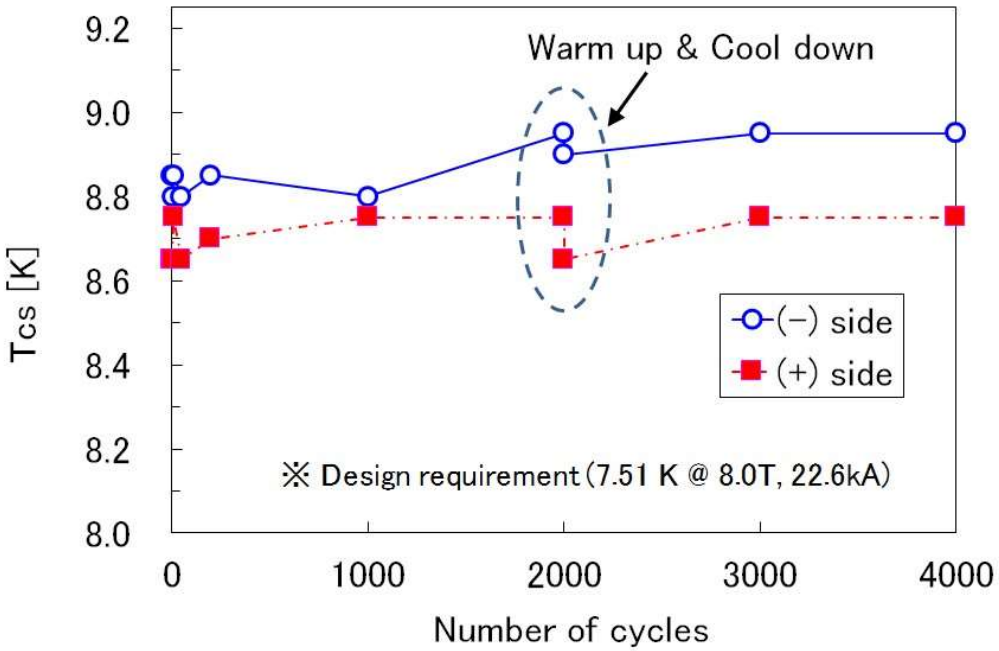

Fig. 26 Tcs measurement results of the CS conductor sample under the EM and thermal cycles.

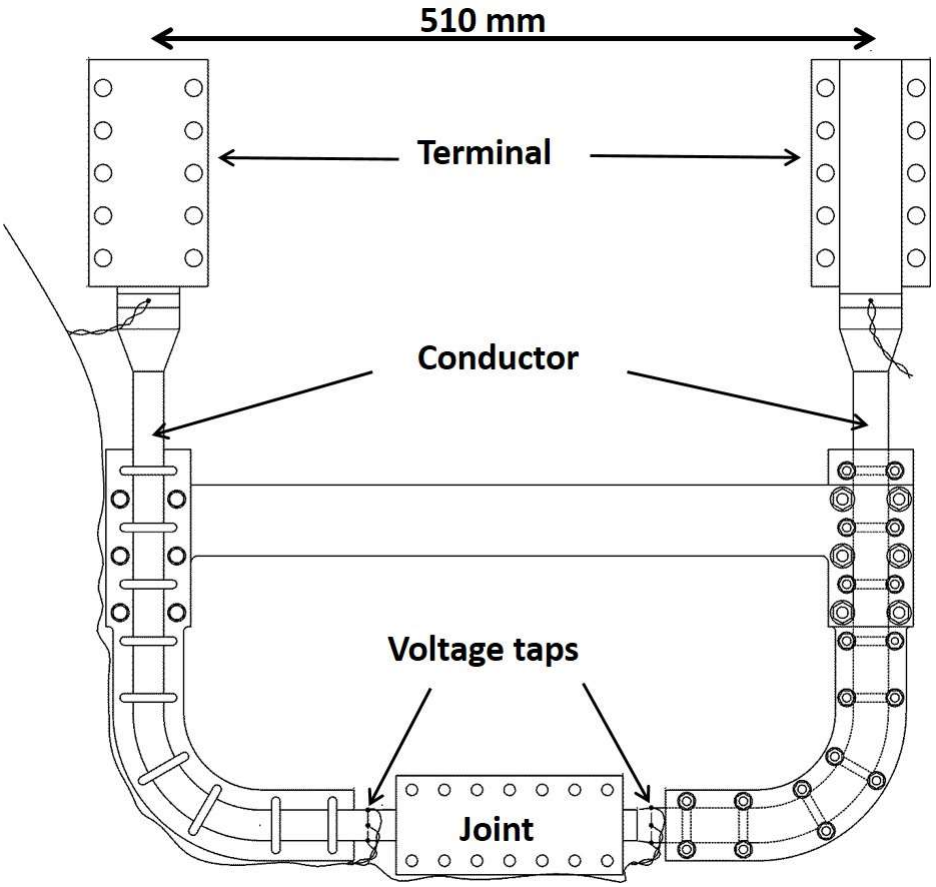

Fig. 27 Schematic view of the prototype joint sample.

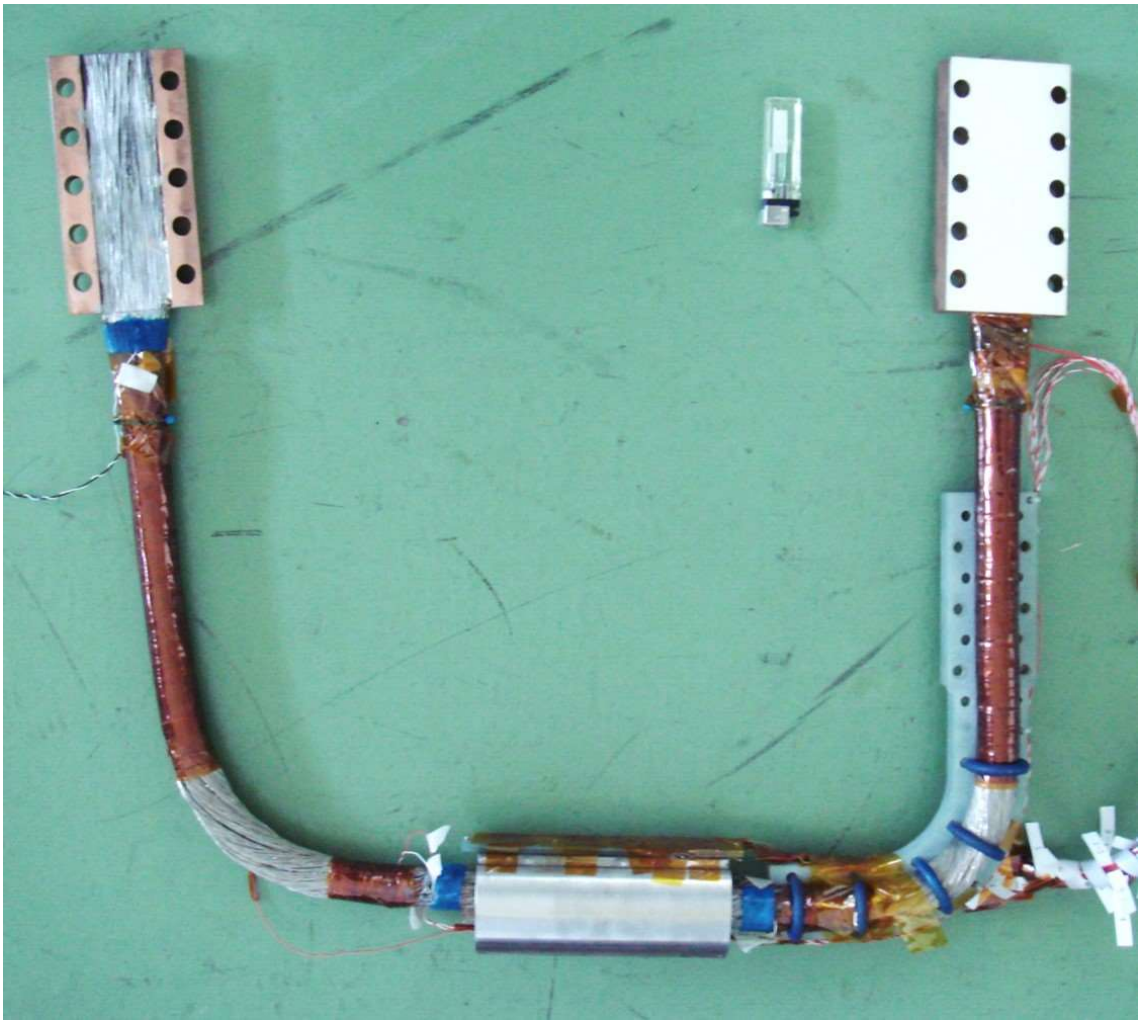

Fig. 28 Photograph of the prototype joint sample.

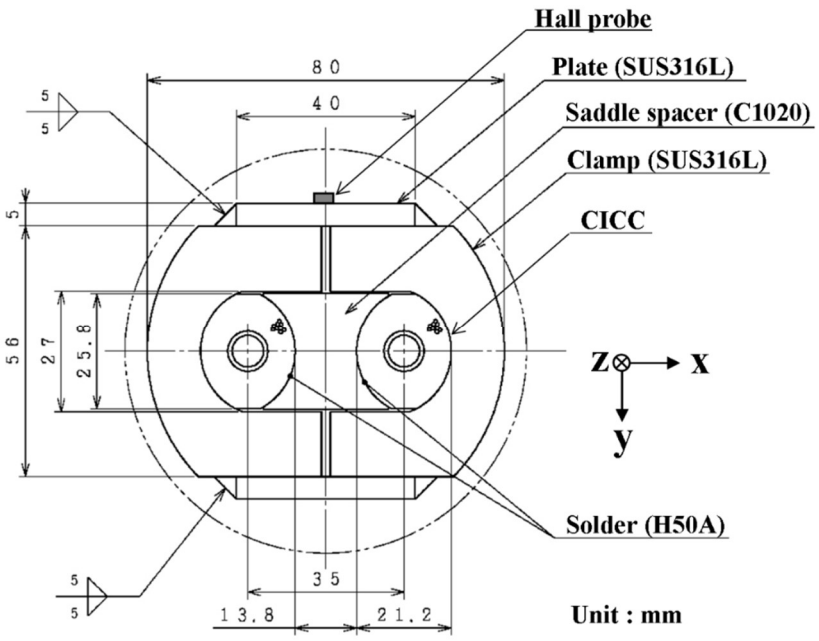

Fig. 29 Cross-section of the prototype joint.

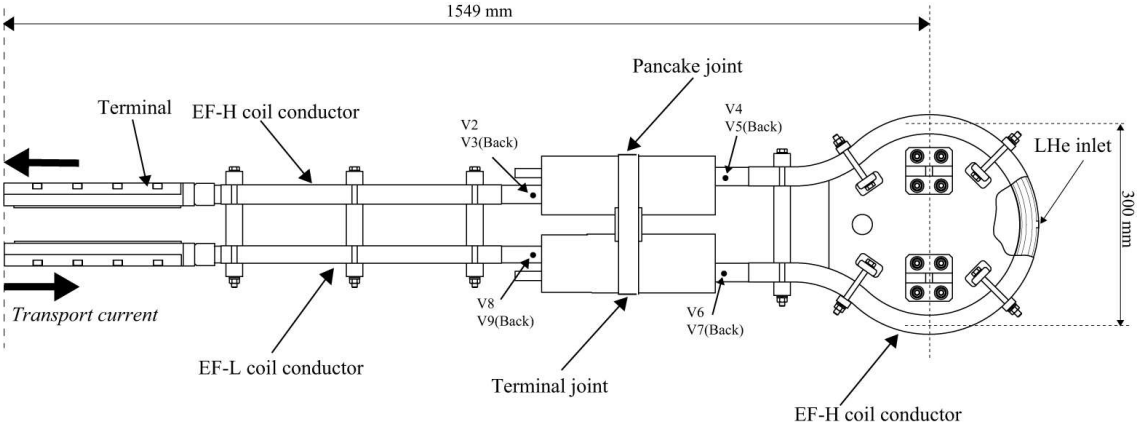

Fig. 30 Schematic view of the pancake and terminal joint sample for the EF coil.

Fig. 31 Photograph of the pancake and terminal joint sample for the EF coil.

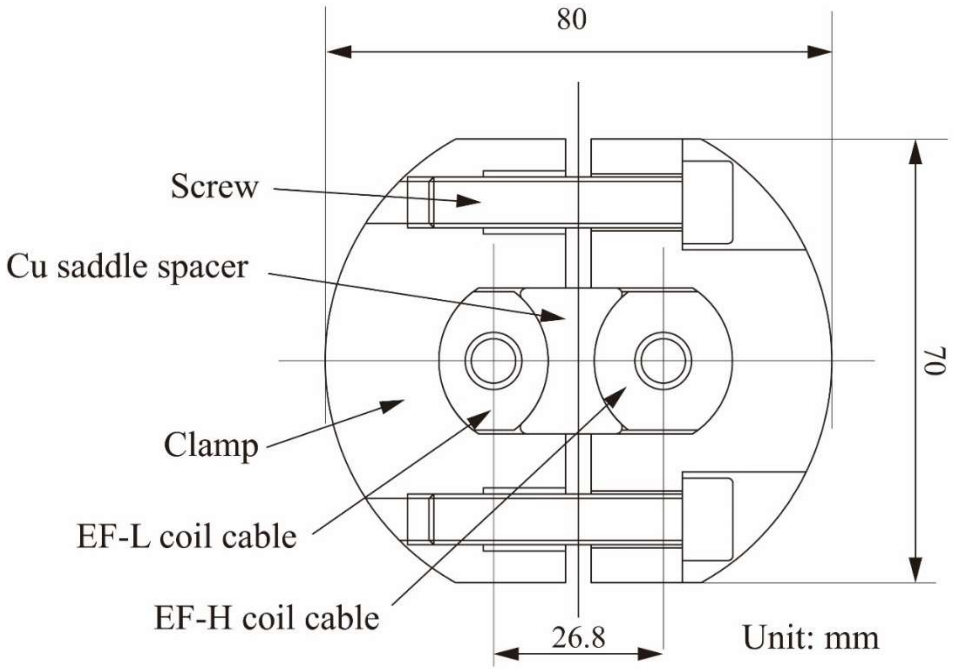

Fig. 32 Cross-section of the pancake joint for the EF coil.

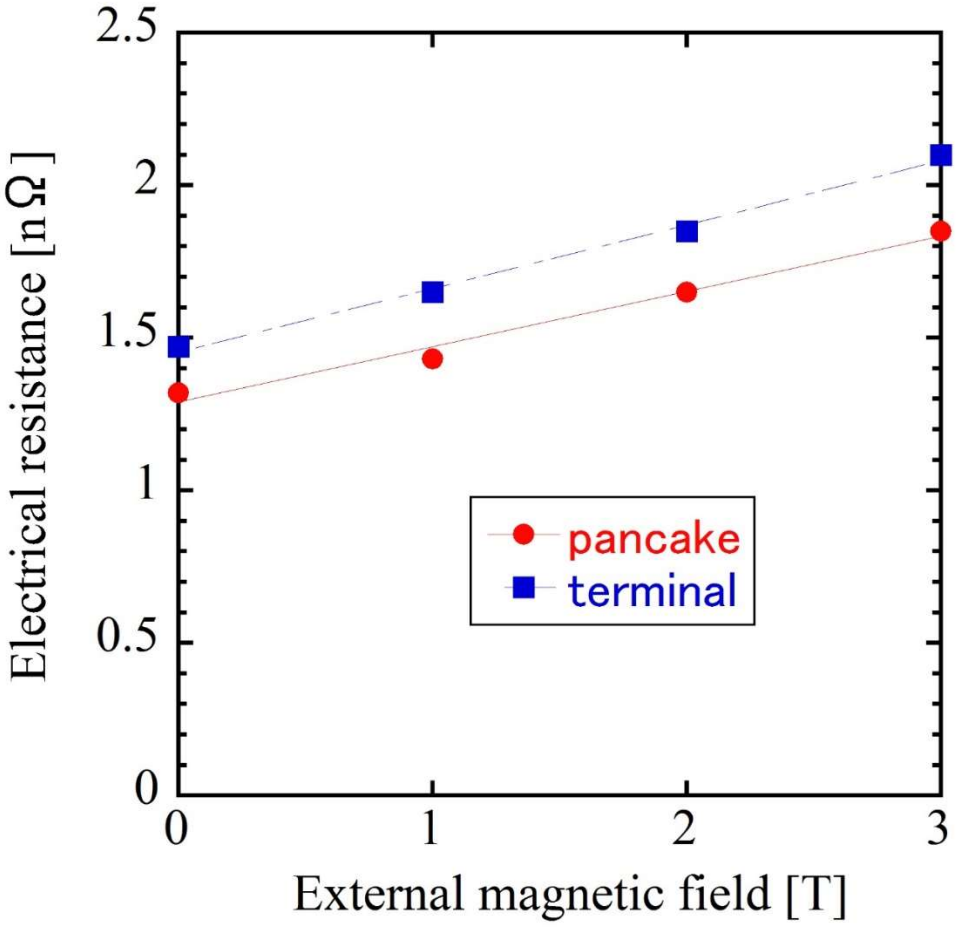

Fig. 33 Joint resistances of the pancake and terminal joints.

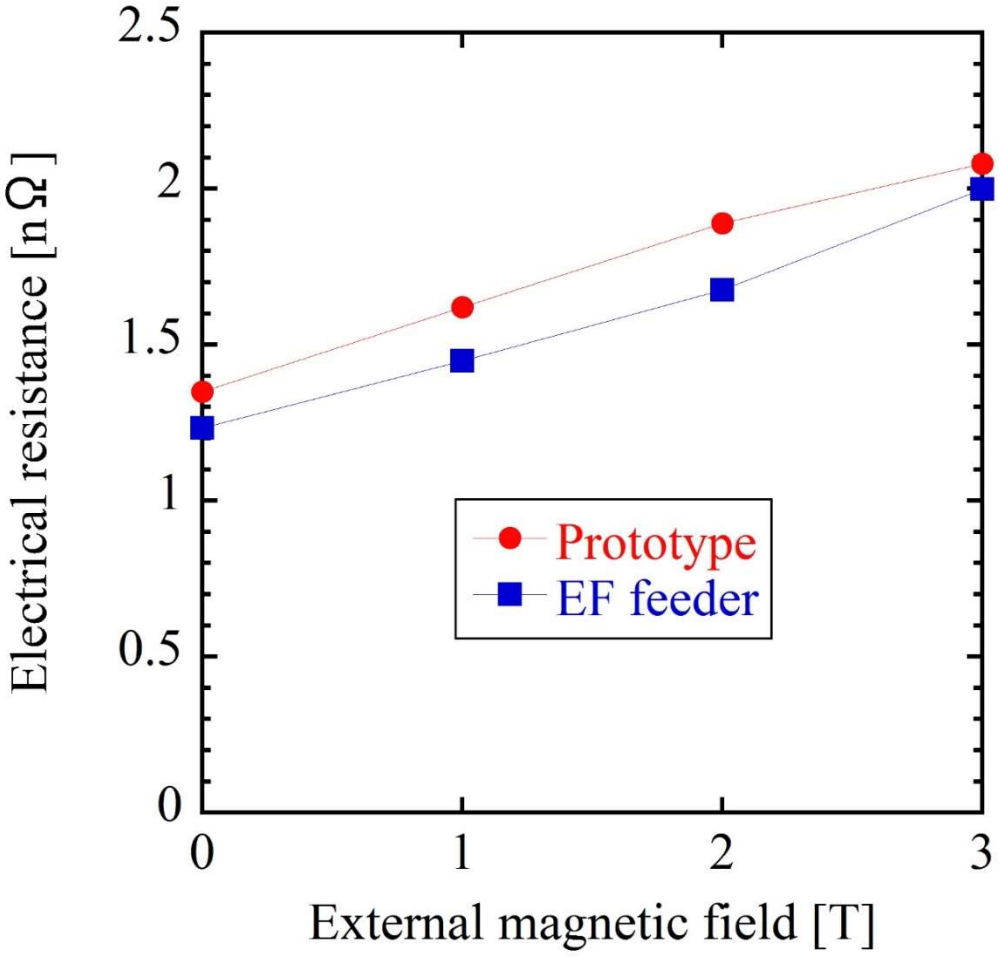

Fig. 34 Joint resistances of the prototype and feeder joints for the EF coil.

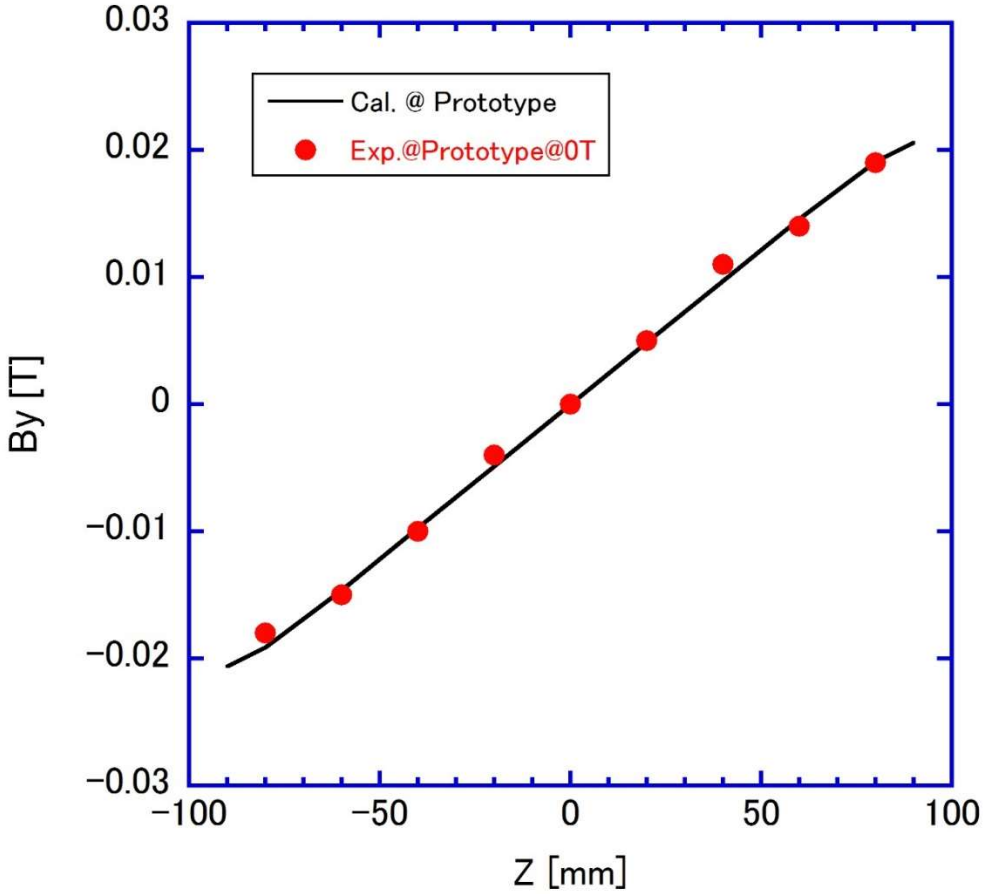

Fig. 35 Measured and calculated self-field of the prototype joint. z = 0 mm is the center of the prototype joint in the longitudinal direction. The position of the Hall sensors is 0 mm in the x direction.

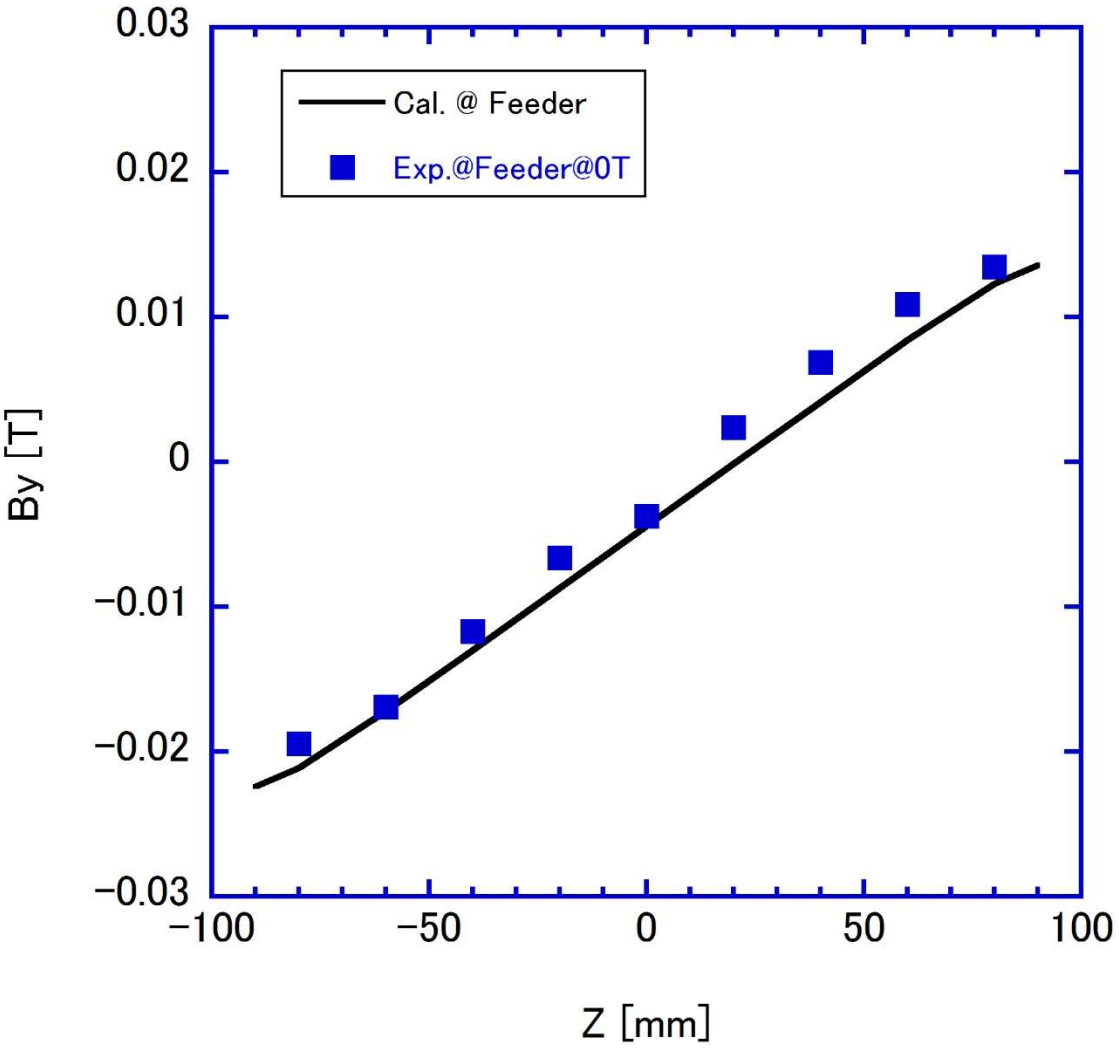

Fig. 36 Measured and calculated self-field of the feeder joint. z = 0 mm is the center of the prototype joint in the longitudinal direction. The position of the Hall sensors is 5 mm in the x direction.

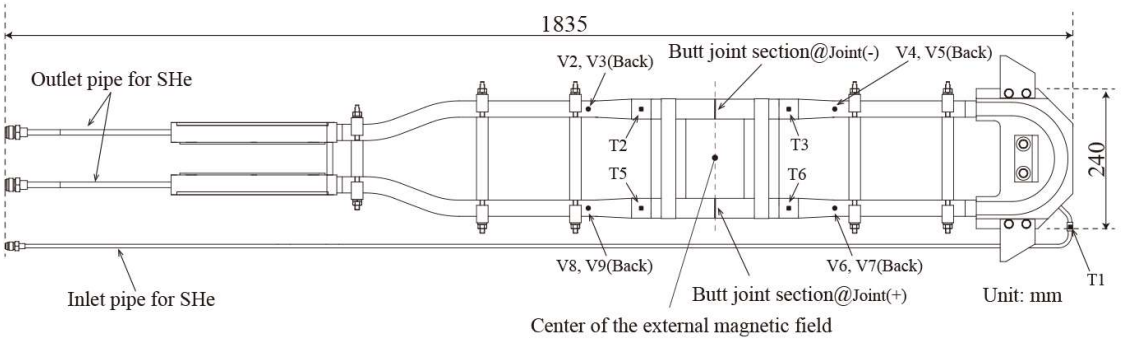

Fig. 37 Schematic view of the pancake joint sample for the CS coil.

Fig. 38 Photograph of the pancake joint sample for the CS coil.

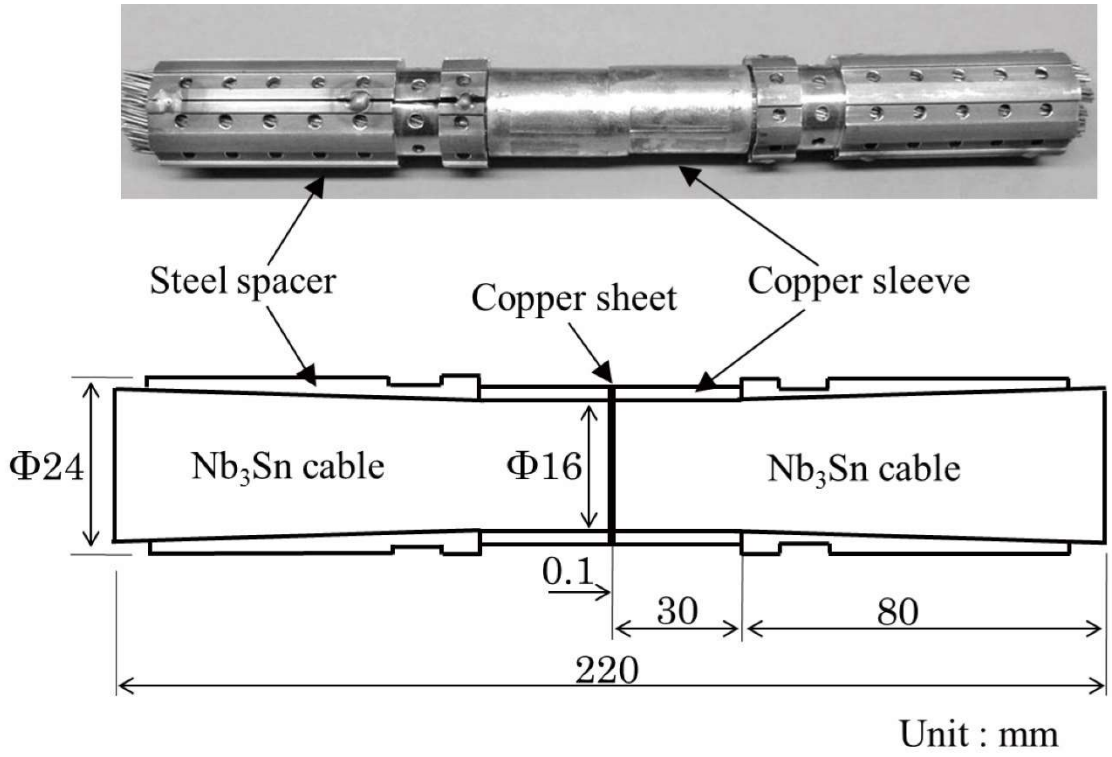

Fig. 39 Configuration and photograph of the butt joint.

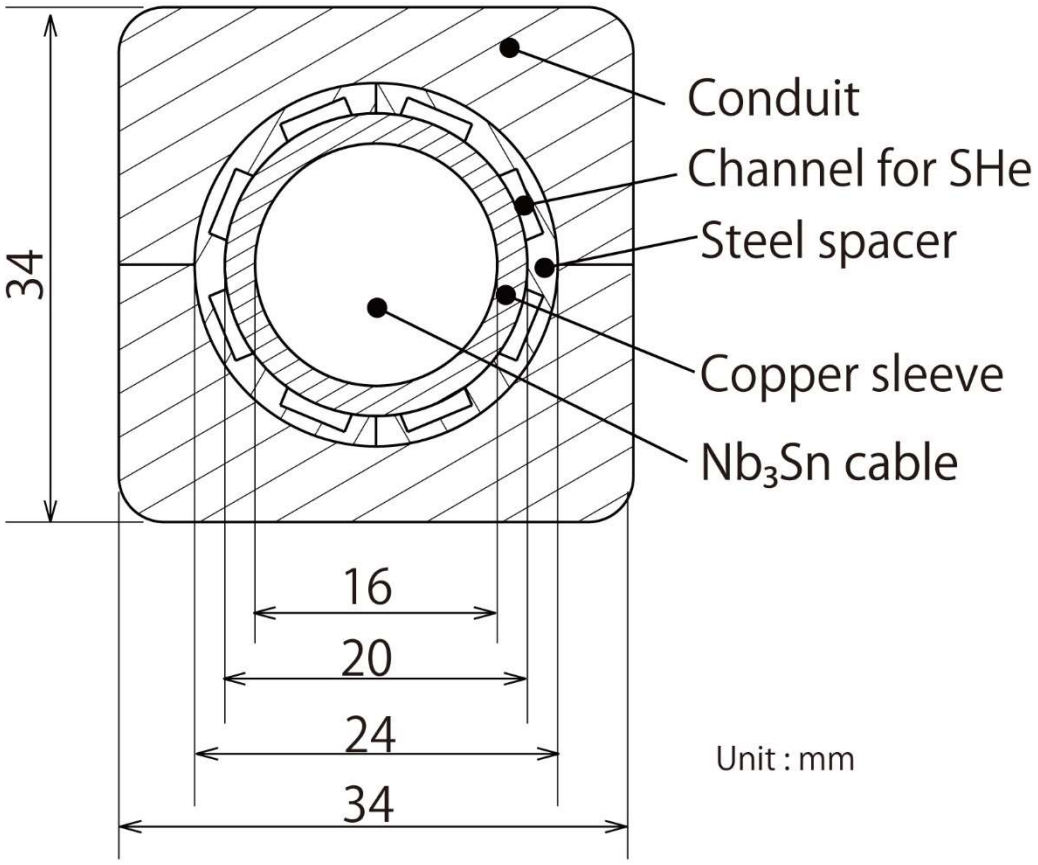

Fig. 40 Cross-section of the butt joint.

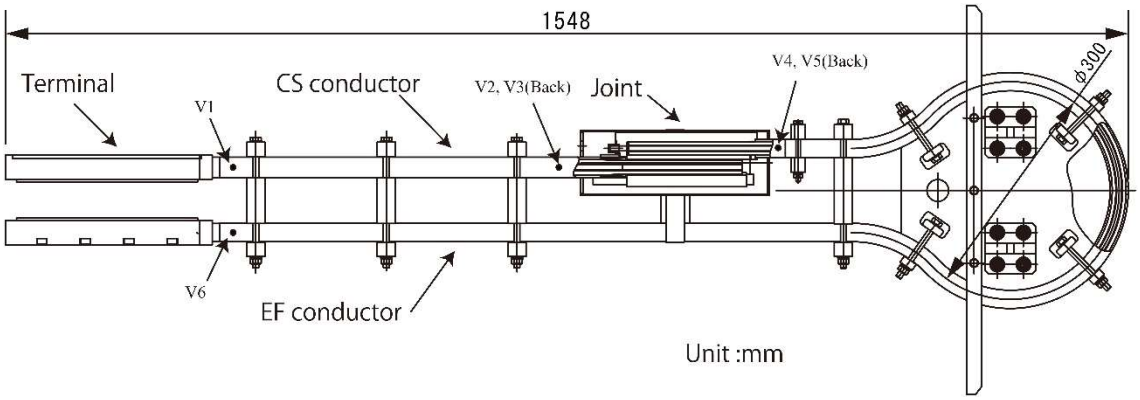

Fig. 41 Schematic view of the terminal joint sample for the CS coil.

Fig. 42 Photograph of the terminal joint sample for the CS coil.

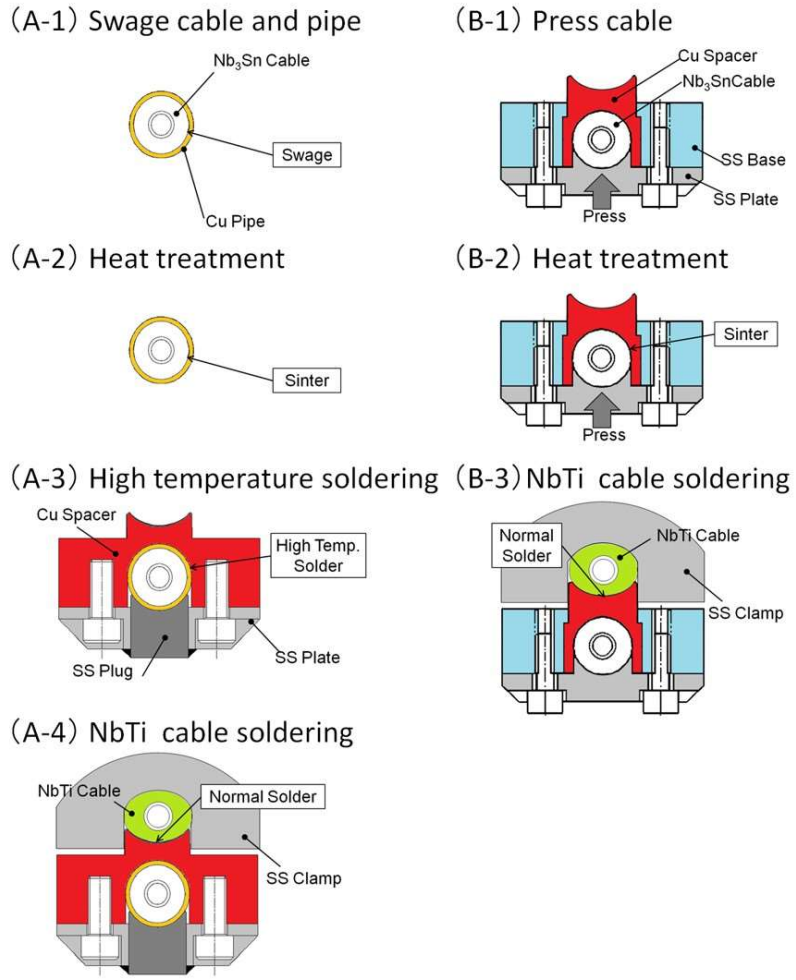

Fig. 43 Fabrication process of the “Type A” and “Type B” joint for the terminal joints.

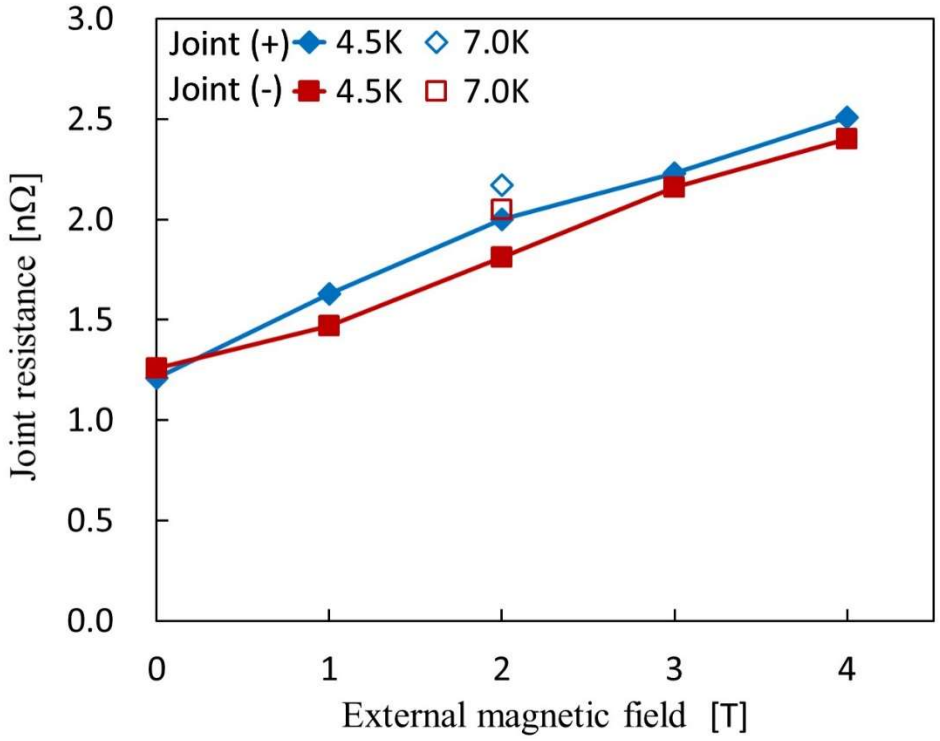

Fig. 44 Joint resistances of the pancake joint for the CS coil.

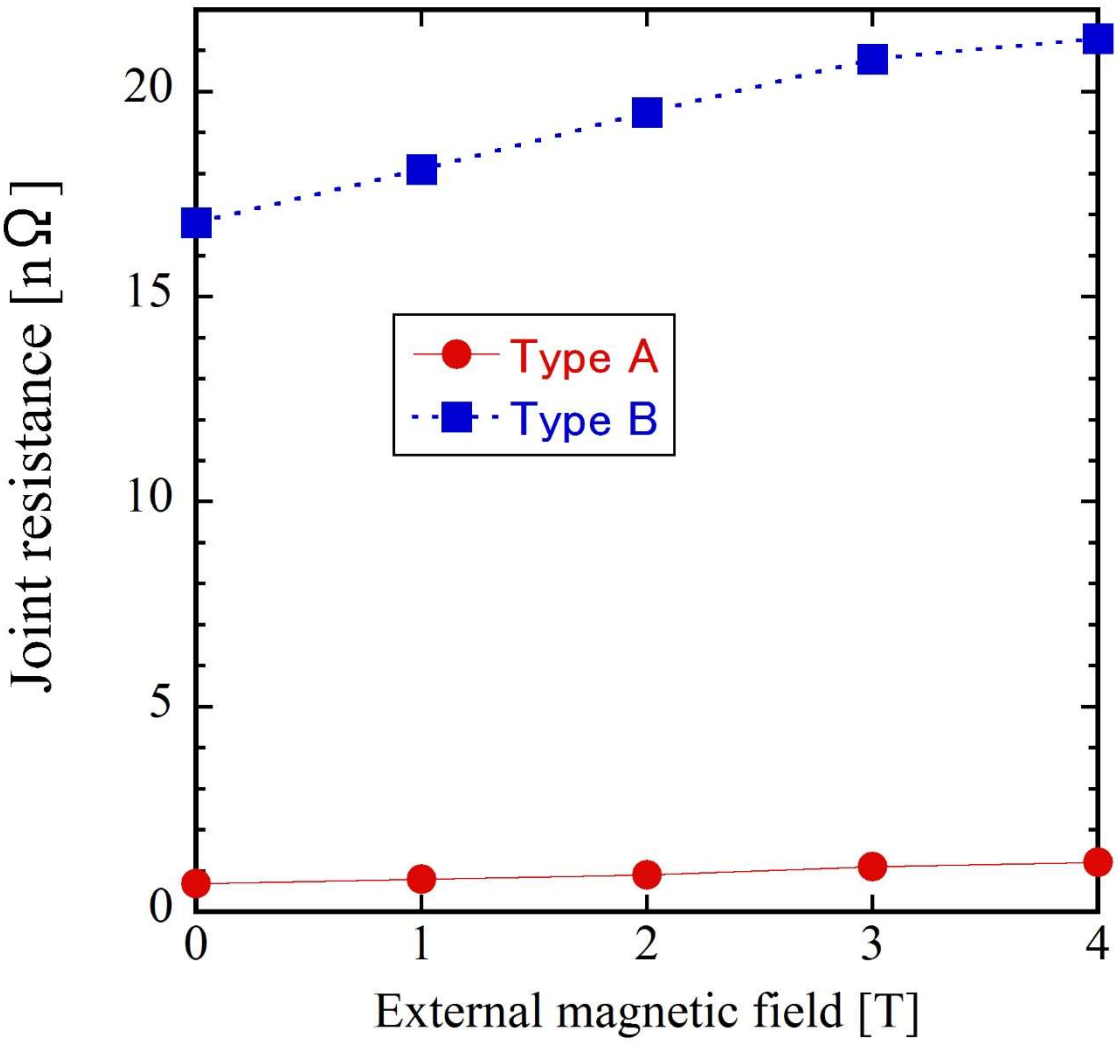

Fig. 45 Joint resistances of the terminal joints for the CS coil.

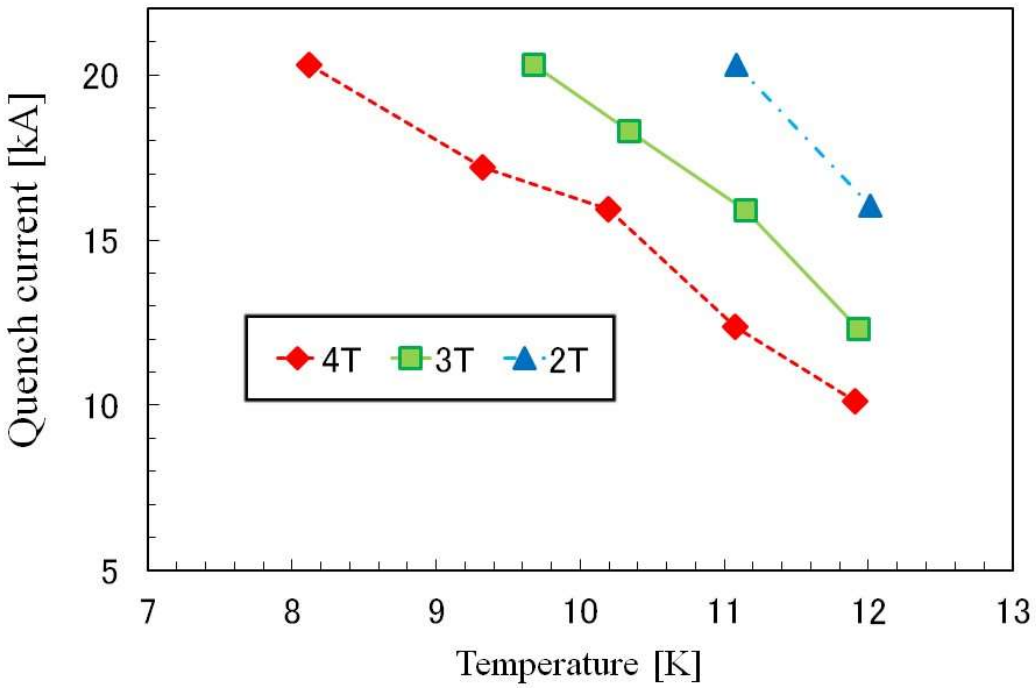

Fig. 46 Quench test results of the pancake joint for the CS coil.

Table 1 Test contents in the collaborative project between JAEA and NIFS.

*JFY	Test contents	Reference
2007	Tcs measurement of a prototype conductor sample for the EF coil	5,6,17
2008	Joint resistance measurement of a prototype joint sample for the EF coil	13
2009	Stability test of a prototype conductor sample for the EF coil	15,16
	Tcs measurement of a conductor sample for the EF-H coil	14,18
	Stability test of a conductor sample for the EF-H coil	15,16
2010	Tcs measurement of a conductor sample for the EF-L coil	14,18
	Stability test of a conductor sample for the EF-L coil	16
	Joint resistance measurement of a joint sample for the EF-H and EH-L coils	21
2011	1st Tcs measurement of a conductor sample for the CS coil	19,20
	2nd Tcs measurement of a conductor sample for the CS coil	19,20
2012	Joint resistance measurement of a butt joint sample for the CS coil	23,25
	Quench test of a butt joint sample for the CS coil	23,24
2013	Joint resistance measurement of a terminal joint (Type A) sample for the CS coil	26
2014	Joint resistance measurement of a terminal joint (Type B) sample for the CS coil	26
	Joint resistance measurement of a feeder joint sample for the EF coil	22

*JFY : Japanese fiscal year

Table 2 Overview of the conductor tests.

	EF Prototype	EF-H	EF-L	CS
Superconducting strand	NbTi	←	←	Nb_3Sn
Test conditions				
Current [kA]	20	←	←	22.6
Magnetic field [T]	6.2	←	4.8	8.0
Mass flow [g/s]	3.9	4.0	4.4	3.4 (before **the cycle) 2.9 (after the cycle)
****Tcs***				
Requirement [K]	−	5.82	6.14	7.51
Test result [K]	6.2	6.21	7.24	8.75 (before the cycle) 8.85 (after the cycle)

*Tcs is an abbreviation for current sharing temperature.

**The cycle is an abbreviation for repeated electromagnetic and thermal cycles.

Magnetic field includes an external field by a split coil and a self-field by a conductor test sample

Table 3 Overview of the conductor joint tests.

	EF Prototype	EF Pancake	EF Terminal	EF Feeder	CS pancake	CS Terminal (Type A)	CS Terminal (Type B)
Joint Type	Lap joint	←	←	←	Butt joint	Lap joint	←
Jointed cables	NbTi cables	←	←	←	Nb_3Sn cables	NbTi / Nb_3Sn cables	←
Test conditions							
Current [kA]	20	←	←	←	←	←	←
Temperature [K]	4.2	←	←	←	7.0	4.2	←
Magnetic field [T]	2	3	←	2	2	4	←
Cooling	Bath	←	←	←	Forced flow	Bath	←
Mass flow rate [g/s]	–	–	–	–	3.3~3.6	–	–
Joint resistance							
Requirement [nΩ]	–	5.0	←	←	←	←	←
Test result [nΩ]	1.9	1.9	2.1	1.7	2.1	1.2	16.8

Table 4 Main parameters of conductor samples for the EF coil.

	Prototype	EF-H	EF-L
Strand diameter [mm]	0.829	←	←
Strand surface	Ni plating	←	←
Plating thickness for strand [μm]	2.5	←	←
Cu/non-Cu ratio	1.95	2.3	←
Number of NbTi strands	486	450	216
Number of Cu wires	0	←	108
Cabling pattern	3×3×3×3×6	3×5×5×6	(2 +1Cu) ×3×6×6
Twist pitch [mm]	45/85/125/160/245	45/85/125/160	←
Sub-wrapping	w/	w/o	w/o
Void fraction [%]	30-32	34	34
Jacket inner size [mm×mm]	22.6×22.6	21.8×21.8	19.1×19.1
Jacket outer size [mm×mm]	28.0×28.0	27.7×27.7	25.0×25.0
Jacket material	SS316L	←	←
Central spiral (id/od) [mm]	7/9	←	←

Table 5 Main parameters of CS conductor.

Strand diameter [mm]	0.82
Strand surface	Cr plating (1.6 μm)
Cu/non-Cu ratio	1.0
Number of NbTi strands	216
Number of Cu wires	108
Cabling pattern	(2 +1Cu) ×3×6×6
Twist pitch [mm]	45/85/125/160
Sub-wrapping	w/o
Void fraction [%]	34
Jacket outer size [mm×mm]	27.9×27.9
Cabling diameter [mm]	21.0
Central spiral (id/od) [mm]	7/9

Table 6 Specifications of the JT-60SA CS and ITER CS conductors.

	ITER CS	JT-60SA
Nb_3Sn strand diameter [mm]	0.83	0.82
Number of Nb_3Sn strands	576	216
Number of copper wires	288	108
Twist pitch [mm]	45/85/145/250/450	45/85/125/160
Jacket inner diameter [mm]	32.6	21.0
Jacket outer size [mm×mm]	49×49	27.9×27.9
Central spiral (id/od) [mm]	7/9	←
Void fraction [%]	33	34
Sub-wrapping	w/	w/o

Table 7 Details of the test conditions for the JT-60SA CS and ITER CS conductor samples.

	ITER CS [29]			JT-60SA CS
Test conditions of EM cycle				
External magnetic field [T]	10.85	←	←	8.0
Operating current [kA]	48.8	38.3	31.6	22.6
EM load [kN/m]	529	416	343	181
*EM stress [MPa]	10.3	8.1	6.7	5.5
Test results				
Conductor performance	Degradation	←	Nearly-constant	←

*EM stress means EM load [kN/m] divided by one-half of the circumference of a jacket inner.